Universidade de Aveiro Departamento de Biologia

Ano 2014/2015

Susana Margarida da Silva Correia

Alteração da resposta regulatória do Rab7a e do Rab9 no subtipo MM1 e VV2 da doença Creutzfeldt-Jakob

Altered regulatory response of Rab7a and Rab9 in MM1 and VV2 subtype of Creutzfeldt-Jakob disease

Universidade de Aveiro Departamento de Biologia
Ano 2014/2015

Susana Margarida da Silva Correia

Alteração da resposta regulatória do Rab7 e do Rab9 no subtipo MM1 e VV2 da doença Creutzfeldt-Jakob

Altered regulatory response of Rab7a and Rab9 in MM1 and VV2 subtype of Creutzfeldt-Jakob disease

Dissertação apresentada à Universidade de Aveiro para cumprimento dos requisitos necessários à obtenção do grau de Mestre em Biologia Molecular e Celular, realizada sob a orientação científica da Professora Doutora Etelvina Ferreira, Professor auxiliar do Departamento de Biologia da Universidade de Aveiro e da Professora. Doutora Inga Zerr, do departamento de Neurologia da Universidade Georg-August, Göttingen.

Dedico este trabalho aos meus avós João Silva e Teresa Gonçalves por todo o amor e educação que nos deram. Dedico também ao meu padrinho João Luis Silva que é mais de um pai para mim, à minha mãe Madalena Silva e à minha irmã Ângela Correia por todo o apoio que me foi dado ao longo dos anos dos quais sem eles não seria a pessoa que sou hoje.

o júri

presidente

Prof. Doutor Helena Silva
Professor Auxiliar do departamento de Biologia da Universidade de Aveiro

Prof. Doutor Etelvina Maria de Almeida Paula Figueira
Professor Auxiliar do departamento de Biologia Etelvina Figueira da Universidade de Aveiro

Prof. Doutor Sandra Maria Tavares da Costa Rebelo
Professor Auxiliar Convidada da Secção Autónoma das Ciências da Saúde da Universidade de Aveiro

agradecimentos

A realização desta dissertação de mestrado contou com importantes apoios e incentivos sem os quais não se teria tornado uma realidade e aos quais estarei eternamente grata.

À Professora Doutora Inga Zerr, do departamento de Neurologia da Universidade Georg-August, o meu agradecimento pela oportunidade de ingressar no seu grupo de investigação.

Ao Doutor Franc Llorens e Matthias Schmitz, do departamento de Neurologia da Universidade Georg-August, o meu profundo agradecimento pela amizade e apoio que me deram ao longo deste ano.

À Professora Doutora Etelvina Figueira, orientadora da tese de mestrado, o meu agradecimento pelo apoio, preocupação e disponibilidade ao longo do ano.

À Professora Doutora Maria de Lourdes Gomes Pereira, Professora associada com agregação da Universidade de Aveiro, o meu agradecimento pela preocupação e disponibilidade ao longo deste ano.

Aos meus familiares o meus profundos agradecimentos por todo o apoio e motivação despendidos.

palavras-chave

CJD-MM1, Rab7, Rab9, PrP^{c}, PrP^{Sc}.

resumo

O presente estudo foi levado a cabo com o intuito de identificar possíveis proteínas que interajam com PrP^{C} que possam fornecer novos conhecimentos sobre as suas funções fisiológicas assim como no papel patológico. O presente estudo incidiu na investigação dos níveis das proteínas endossomais Rab7a e Rab9 em amostras do córtex frontal e cerebelo de pacientes diagnosticados com sCJD-MM1 e sCJD-VV2. Observamos um aumento significativo dos níveis intracelulares do Rab7a em pacientes diagnosticados com sCJD-MM1 e sCJD-VV2 quando comparadas com amostras de pacientes na mesma faixa etária sem a doença (controlo). As interações entre PrP^{C} e as proteínas Rab7a e Rab9 foram posteriormente estudadas com o auxílio à microscopia confocal. Os resultados da imunofluorescência sugeriram potenciais interações entre as proteínas Rab7a com o PrP^{C}. O siRNA-Rab7 foi usado para diminuir a expressão da proteína Rab7a ("Knockdown") na cultura primária de células do córtex de ratos saudáveis. Na cultura de células do córtex tratadas com o siRNA-Rab7, foi observado um emparelhamento da via endocítica. Seguidamente investigamos possíveis interações da proteína Tau com a proteína Rab7a, recorrendo ao western blot e a microscopia confocal. Culturas de células do córtex de ratos saudáveis foram tratadas com siRNA-Tau, siRNA-Rab7a e siRNA. Os resultados da imunofluorescência das diferentes culturas celulares sugeriram uma potencial interação entre as proteínas Tau e Rab7a. Nas linhas celulares tratadas com siRNA-Tau os níveis intracelulares das proteínas Rab7a e Rab9 aumentaram significativamente, assim como, foi também observada a alteração da sua localização. Nas células tratadas com siRNA-Rab7a observamos uma diminuição da acumulação da proteína Tau na região citosólica. Em conclusão, este trabalho pode ajudar a perceber e a caracterizar a progressão da doença nos subtipos específicos, no caso de sCJD. Contudo, este trabalho poderá ser também um passo à frente para o desenvolvimento de novas estratégias terapêuticas para os subtipos sCJD-MM1 e sCJD-VV2.

keywords CJD-MM1, Rab7, Rab9, PrP^{c}, PrP^{Sc}.

abstract The present study was undertaken to identify proteins interacting with PrP^{C} that could provide new insights into its physiological functions and pathological role. We performed a target search for lysosomal network protein, Rab7a and Rab9, in frontal cortex and cerebellum of human brain from patients with sCJD-MM1 and sCJD-VV2. The intracellular level of Rab7a was increased significantly, when compared with healthy age-matched control. Interactions of PrP^{C} and Rab7a/Rab9 were further investigated by using confocal laser scanning microscopy. Immunofluorescence results suggested potential interactions of Rab7a and PrP^{C}. siRNA against the Rab7a gene was used to knockdown the expression of Rab7a protein in primary cell culture of cortical neurons from wild type mice. This depleted Rab7a resulted an impairment of PrP^{C} trafficking leading to an accumulation of PrP^{C} in the endocytosis pathway. Furthermore, interactions of Tau and Rab7a were investigated by using western blot analysis and confocal laser scanning microscopy. Cell cultures of cortex of wildtype mice were treated with siRNA-Tau, siRNA-Rab7 and control siRNA followed by immunofluorescence. The results of immunofluorescence suggested potential interaction of Tau and Rab7a. Cells lines treated with siRNA-Tau, the intracellular levels of Rab7a and Rab9 significantly increases and their localization is also modified. When we transfected this cells lines with siRNA-rab7a the accumulation of Tau decreases in cytosolic region and their localization was also modified when compared with control cells. In conclusion, this study may help to understand and characterize the subtype specific disease progression in CJD cases. Furthermore, it could be a step ahead to development of new treatment strategies for diseases subtype specific manner.

Index

List of Figures

List of Tables

Abbreviations

^{o}C	Celsius
µg	Microgram
µl	Microliter
µm	Micro meter
aa	Amino acid
AD	Alzheimer’s disease
ATP	Adenosine triphosphate
BFA	Brefeldin A
bp	Base pair
BSA	Bovine serum albumin
BSE	Bovine spongiform encephalopathy
CSF	Cerebrospinal fluid
dH20	Distilled water
ddH2O	Double distilled water
DMEM	Dulbecco's Modified Eagle Medium
DTT	Ditiotreitol
ECL	Enhanced chemiluminescence
ER	Endoplasmic reticulum
ERAD	Endoplasmic reticulum associated degradation
ERGIC	ER–Golgi intermediate compartment
FBS	Fetal bovine serum
FCS	Fetal calf serum
h	Hour
IAA	Iodoacetamide
kDa	Kilodalton
M	Mol
mg	Milligram
min.	Minute
ml	Milliliter
PBS	Phosphate buffered saline
PVDF	Polyvinylidene fluoride

PrP^{C}	Cellular prion protein
PrP^{SC}	Infectious isoform of prion protein
rpm	Revolutions per minute
Rab7a	Ras-related protein Rab-7a
Rab9	Ras-related protein Rab-9
RT	Room temperature
s	second
sCJD	Sporadic Creutzfeldt-Jakob disease
SDS-PAGE	Sodium Dodecyl Sulphate Polyacrylamide Gel Electrophoresis
siRNA	Small interfering RNA
TBS	Tris buffered saline
TBST	TBS with 0.1% Tween
TE	Tris EDTA
TEMED	N, N, N´, N´-tetramethylethylenediamine
Tris	Tris-(hydroxymethyl)-aminomethane
TSEs	Transmissible spongiform encephalopathies
WB	Western blot

I Introduction

1 Cellular prion protein (PrP^C)

The cellular form of the prion protein (PrP^C) is a glycosyl-phosphatidyl-inositol (GPI)-anchored glycoprotein, highly expressed in the neurons of the brain and spinal cord region (Stahl et al. 1987). However, the physiological function of PrP^C is still not clear, in recent years, some putative functional aspects were attributed to PrP^C, synaptic regulatory response (as a receptor or receptor-related in $GABA_A$-ergic inhibitory synapses) (Puoti et al. 2012), sleep and circadian rhythms regulator, inhibitory regulation of N-methyl-D-aspartate (NMDA) receptors, interaction with stress inducible protein 1 (STI1), regulation of cell differentiation and apoptosis, maintenance of peripheral nerve myelin, role in neuronal growth and survival (protection against bax-mediated cell death); signal transduction (caveolin1-dependent coupling to tyrosine kinase Fyn); signaling receptor (binding to neural cell adhesion molecule); oxidative stress, copper binding (cooper serving as a cofactor for an undetermined PrP^c enzyme activity) (Lorca et al. 2011; Martins et al. 2010), receptor for amyloid beta in Alzheimer's disease and possibly for other amyloids (Laurén et al. 2009; Resenberger et al. 2011) and it is known that the conformal change of PrP^c can cause serious neurodegenerative diseases (Nicolas et al. 2009).

The PrP^c is synthesized in the endoplasmic reticulum (ER), processed in golgi apparatus and then transferred to the plasmatic membrane in full length form. During its synthesis the cellular prion can take various forms in the ER. The PrP^c can be found at least in two transmembrane topologies (Hegde & Lingappa 1999):

1. ^{ctm}PrP = The ^{ctm}PrP form is when the c-terminal of PrP^c is in the ER lumen,

2. ^{Ntm}PrP = The ^{Ntm}PrP form is when the N-terminius of PrP^c is in the ER lumen (Figure 1).

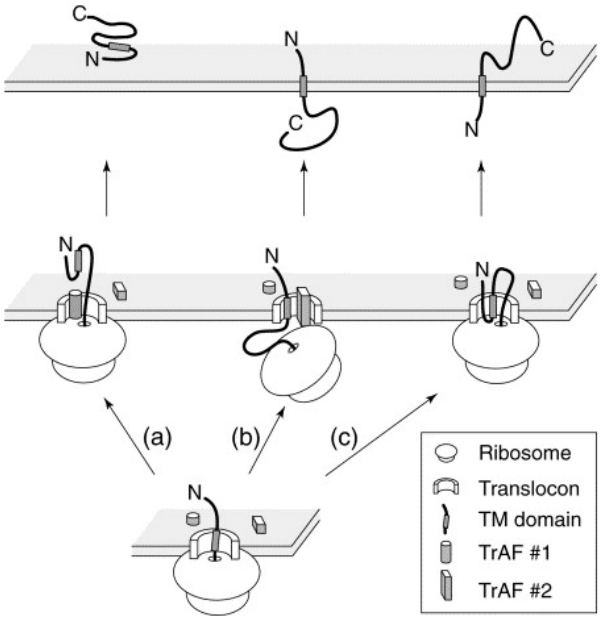

Figure 1. Putative mechanism for generating different topological forms: The PrP^{c} is translocated to the endoplasmic reticulum (ER) by ribosomes. The nascent protein chain containing a transmembrane (TM) domain (shaded rectangle) can have different orientations into the ER membrane. This process depends on a particular translocation accessory factor (TrAF #1) that might shield the hydrophobic TM domain from being recognized by the translocon, allowing it to be translocated into the ER lumen leading to cyPrP form. If TM domain is recognized by translocation machinery ((b) or (c)), another translocation accessory factor (TrAF #2) interacts with nascent chain leading to ^{Ntm}PrP form (b) or if there is no interaction of the translocation accessory factor (TrAF #2) with, the nascent chain, the least energetically demanding orientation, is favoured the ^{ctm}PrP form (c). The final topology resulting from each of these possibilities is shown at the top of the diagram (Take from Hegde e Lingappa, 1999).

The transportation of PrP^{c} leads to unglycosylated and glycosylation (mono- and di- glycosylated) forms formed in RE and it is transported to the golgi apparatus for further modifications (Figure 2). Therefore the cellular prion is transported to the cellular membrane under its mature form, PrP^{c} (Harris 2003). The PrP^{c} can still be found in the cytosol, cyPrP. The cyPrP can be the result of controlled mechanisms of ER. When the protein is misfolded or under ER stress conditions, proteins undergo retrograde transport to the cytosol, become polyubiquitinated, and are degraded by the proteasome through a process called ER-associated degradation, ERAD (Lin et al. 2013).

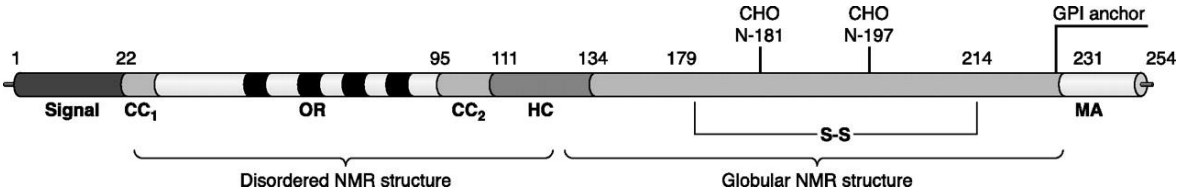

Figure 2. Primary structure of PrP^c including posttranslational modifications: A secretory signal peptide resides at the extreme NH_2 terminus. CC_1 and CC_2 define the charged clusters. OR indicates the octapeptide repeat, and four are present. HC defines the hydrophobic core. MA denotes the membrane anchor region. S-S indicates the single disulfide bridge, and the glycosylation sites are designated as CHO. The numbers describe the position of the respective amino acids (Take from Aguzzi e Calella, 2009).

1.1 Structure of cellular prion and prion disease

The structure of PrP^c is composed of three regions; alpha-helix (~ 40% of protein) separated by loop/turn regions and by two small regions of beta-sheet (~ 3% of protein). This conformation of PrP^c is sensitive to proteolysis, PrP-sen. However, when PrP^c undergoes structural changes, it leads to the increase of beta-sheets ~ 40%, and PrP^c becomes misfolded and resistant to proteases attack, PrP-res (Prusiner 2004; Novakofski et al. 2005).

The conversion of PrP-sen to PrP-res can occur when PrP-res binds to PrP^c or when the PrP-sen conformation is altered into PrP-res by a poorly understood pathway (Figure 3). Its conversion on the cell surface leads to PrP-res accumulation extracellularly, and along endocytic pathway leads to accumulation of PrP-res in the lysosome (Moore et al. 2009; Lee et al. 2013). The accumulation of PrP-res in the lysosomes leads eventually to lysosome´s burst and the release of all lysosomal enzymes together with the PrP-res in the cytoplasm, leading to cells apoptosis (Araújo 2013).

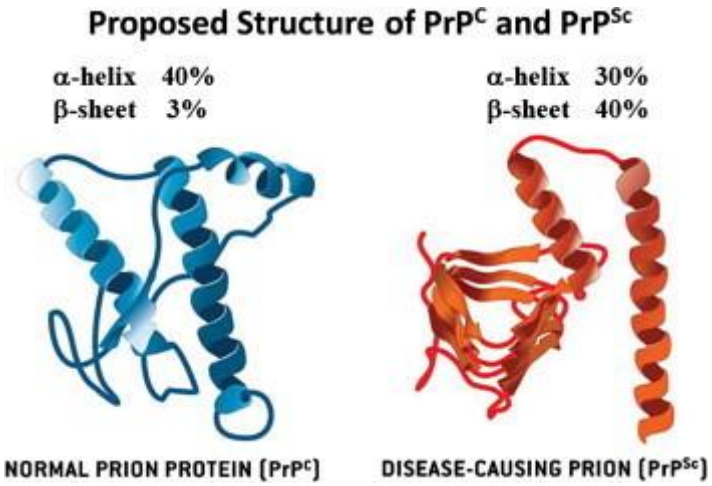

Figure 3. Structure of PrP^{c} and PrP^{Sc}: Normal and disease-causing prions structures (Take from Lee *et al.*, 2013).

1.2 PrP-res form and prion diseases

PrP-res accumulates intra and/or extracellularly leading to the neurodegenerative diseases called transmissible spongiform encephalopathies (TSEs),also called prion diseases. The aggregates of PrP-res yield neurological dysfunctions and cells death. The brain lost neurons and with advancing disease the brain looks like a sponge form leads to death in humans and other mammals (Belay 1999). In mammals, the TSE occurs as scrapie disease (sheep), transmissible mink encephalopathy (mink), chronic wasting disease (deer), bovine spongiform encephalopathy (cattle) and feline spongiform encephalopathy (cats). The most common prion disease present in humans is Creutzfeldt-Jakob disease (Lee et al. 2013; Moore et al. 2009).

Table 1. Transmissible spongiform encephalopathies (TSEs) in humans and animals (Liemann & Glockshuber 1998; Puoti et al. 2012)**.**

Disease name	Animal species	Etiology
Scrapie	Sheep	Infection
Transmissible mink encephalopathy	Mink	Infection
Chronic wasting disease	Deer	Infection
Bovine spongiform encephalopathy	Cows	Infection

Feline spongiform encephalopathy	Cats	Infection
Bovine spongiform encephalopathies	Cattle	Infection
Creutzfeldt-Jakab disease Iatrogenic Sporadic Inherited New variant	Humans	 Infection Unknown Mutation in PrP gene Infection from bovine prion?
Gerstmann-Stränssler-Scheinker syndrome	Humans	Mutation in PrP gene
Fatal familial insomnia	Humans	Mutation in PrP gene

2 Creutzfeldt-Jakob disease (CJD)

The sporadic Creutzfeldt Jakob disease (sCJD) is the most common form of prion disease (85% to 95%) of all human prion disease (Ladogana et al. 2005; Masters et al. 1979). In sCJD, the source of contamination is unknown. The disease is not associated with any mutation in *PRNP* allele or by any exposure to Prion disease. However, studies have been documented that people with a medical history of psychosis, family history of CJD, history of multiple surgical procedures and residence for more than 10 years on a farm have a significant risk to develop sCJD (Villemeur 2013).

The sCJD is the prion disease with the highest degree of phenotypic heterogeneity. This phenotype heterogeneity has been associated with polymorphisms of codon 129 of the prion protein gene (*PRNP*) and to the size of protease resistant core of the prion protein (PrP^{Sc}), ~21 KDa (type 1) and ~19KDa (type 2). The codon 129 of *PRNP* consists in an amino acid methionine (M) or valine (V) in each allele. The the resistant core of PrP^{Sc} patient genotype can be MM, MV or VV with type 1 or type 2 of and therefore, they have a different phenotype of prion disease (Figure 4) (Parchi, Capellari, et al. 1999). The sCJD is subdivided in 6 subtype, sCJD MM1, sCJD MM2, sCJD MV1, sCJD MV2, sCJD VV1 and sCJD VV2. And these subtypes were grouped in two groups, sCDJ cognitive type and sCDJ ataxic type. Each group and subtypes are characterized

by different clinical and histopathological features (Cali et al. 2009; Puoti et al. 2012).

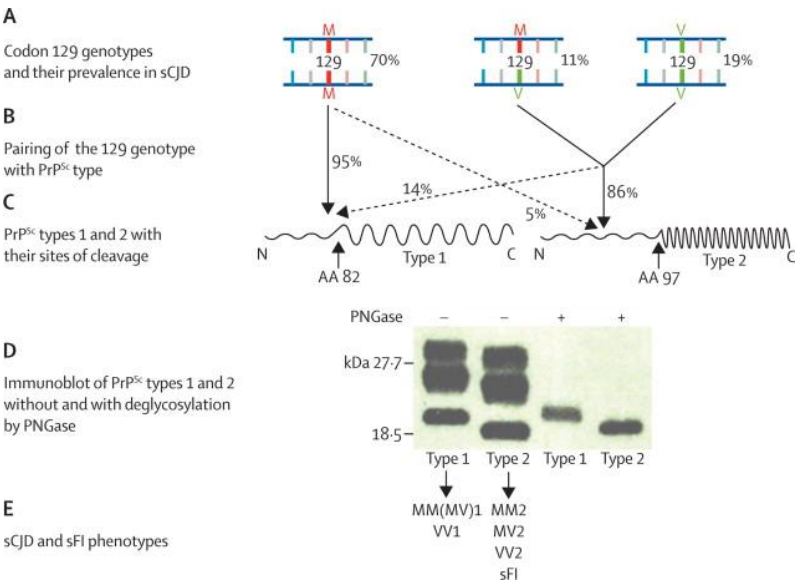

Figure 4. Correlations between the PrP genotype, as determined by the MV polymorphism at codon 129, and PrP^{Sc} types 1 and 2: (A) Diagrammatic representation of each of the three 129 genotypes (MM, MV, and VV) with their average relative prevalence in all subtypes of sCJD. **(B)** PrP^{Sc} type 1 is associated with the 129MM genotype in about 95% of cases, whereas MV and VV genotypes are associated with PrP^{Sc} type 2 in about 86% of cases. **(C)** Diagrammatic representation of PrP^{Sc} types 1 and 2; each consists of an amino-terminal region (N) of different sizes that is protease-sensitive and is digested down to amino acid (aa) 82 in type 1 and to amino acid 97 in type 2 (arrows). The different cleavage site is thought to be the result of the different conformation in PrP^{Sc} types 1 and 2. **(D)** Types 1 and 2 PrP^{Sc} have distinct electrophoretic mobilities because of the different size of their respective protease-resistant fragments (type 2 being smaller than type 1) and are easily distinguished by their different migration on electrophoresis, especially after cleavage of the sugars by the enzyme peptide N glycosidase F (PNGase). **(E)** Both 129 genotype and PrP^{Sc} types are thought to act as determinants of the phenotypes of sporadic prion diseases that are commonly identified with letters and numbers to indicate the associated genotype and PrP^{Sc} type. PrP^{Sc}=scrapie prion protein. M=methionine. V=valine. sCJD=sporadic Creutzfeld-Jakob disease. sFI=sporadic fatal insomnia (Take from Puoti *et al.*, 2012).

2.1 sCJD cognitive type

2.1.1 sCJD MM1 and sCJD MV1

These sCJD subtypes account for approximately between 60 to 70% of sCJD cases and are observed in individual with genotype MM or MV at codon 129 of the PrP gene and carrie type 1 of PrP^{Sc}. However, approximately 95% of individuals in this subgroup belong to MM1 genotype in codon 129, while the individuals with genotype MV are rare (Gambetti et al. 2003). The MM1 and MV1 genotype are clinical and histopathology indistinguishable, the difference between both is the 129 genotype. Therefore, the MM1 and MV1 belong to the same subgroup (Takada & Geschwind 2013; Puoti et al. 2012). The mean age onset of disease is around 66 years old and this subtype has a short duration of illness. When patients have severe signs of the disease in a few weeks enter vegetative state and die, the mean duration of the disease is 4 month after onset (Parchi, Giese, et al. 1999; Parchi et al. 2009).

The phenotype associated with subtype MM1/MV1 is characterized by rapidly progressive cognitive decline, as memory loss and confusion/disorientation occasionally accompanied by cortical visual disturbances. In an initial stage the cognitive decline appears in approximately 70% of patients, and in a short time rises to 93%. In this subtype the patients also present ataxia, about 53% percent in advanced stage. Approximately 97% of patients have a spontaneous or induced myoclonus, and mild psychiatric symptoms as depression, anxiety and psychosis (Araújo 2013; Gambetti et al. 2003; Puoti et al. 2012).

The patients with sCJD MM1 phenotype have presence of 14-3-3 protein and Tau in cerebrospinal fluid (CSF) and they are associated with periodic sharp wave complexes (PSWC) on electroencephalogram (EEG). The presence of these three characteristics make a positive diagnostic of sCJD MM1 (Wieser et al. 2006; Gambetti et al. 2003; Puoti et al. 2012).

2.1.2 sCJD 129 MM2

This subtype is very rare and account for 2 to 10% of sCJD cases, is observed in individuals with genotype MM2 at codon 129 of the PrP gene and carry type 2 of PrP^{Sc}. The mean age of disease onset is around 66 years old and

the duration of illness is about 14 months after onset (Bishop et al. 2010; Parchi, Giese, et al. 1999).

The phenotype associated with this subtype is characterized by a cognitive decline in all patients and amnestic aphasia in an initial stage in 32% of patients . Through the course of the illness, amnestic aphasia increases to 72% of patients and the patients occasionally feature pyramidal sings, apraxia, Parkinsonism and myoclonus (Moda et al. 2012; Araújo 2013; Gambetti et al. 2003).

Between 24 to 44% of e patients with sCJD MM2 phenotype have periodic sharp wave complexes (PSWC) on electroencephalogram (EEG) in the intermediate and advanced stages of disease. The 14-3-3 and Tau CFS test are positive in approximately 50% of all cases of sCJD MM2. However, the magnetic resonance imaging (MRI) showed abnormal imaging in most (93%) of patients (Puoti et al. 2012).

2.1.3 sCDJ 129 VV1

This subtype is very rare and account between 1 to 4% of sCJD cases, it is the most uncommon prion disease. This subtype is observed in individuals with genotype VV1 at codon 129 of the PrP gene and carries type 1 of PrP^{Sc}. The mean age onset of disease is around 43 years old and has a long duration of illness, about 19 months after onset. In the initial stage it can be difficult to distinguish from sCJD MM2 subtype. Both subtypes have a cognitive decline and patients can remain mono-symptomatic for several months (Krasnianski et al. 2006; Meissner et al. 2005). However, in patients with sCJD VV1 subtype the cognitive decline is slower than in patients with sCJD MM2 and is occasionally associated with personality changes. Through the course of the illness, all patients feature cognitive decline and patients occasionally feature psychiatric symptoms, pyramidal signs, Parkinsonism and myoclonus (Parchi, Giese, et al. 1999; Meissner et al. 2005).

The patients with sCJD VV1 phenotype have presence of 14-3-3 protein and Tau in cerebrospinal fluid (CSF) and the electroencephalography (EEG) shows non-specific slowing but not periodic sharp wave (PSW) complexes. The

MRI is abnormal in all patients (Gambetti et al. 2003; Puoti et al. 2012; Wieser et al. 2006).

2.2 sCDJ ataxia type

2.2.1 sCDJ VV2

This subtype accounts for approximately 16% of sCDJ cases and is observed in individuals with genotype VV at codon 129 of the PrP gene and carry PrP^{Sc} type 2. The mean age onset of disease is around 64 years old and the duration of illness is about 6 months after onset (Parchi, Giese, et al. 1999; Parchi et al. 2009).

The phenotype associated with this subtype is characterized by ataxia in almost all patients in the initial state of disease. Through the course of the illness, all patients have cognitive decline and ataxia. In this subtype it is also characteristic myoclonus (approximately 66% of patients) and pyramidal signs (50% of patients) (Araújo 2013; Gambetti et al. 2003; Puoti et al. 2012).

The patients with sCJD VV2 phenotype have presence of 14-3-3 protein and Tau in the CSF. The MRI is abnormal in approximately 60% of patients (Puoti et al. 2012).

2.2.2 sCDJ MV2

This subtype accounts for approximately 9% of sCDJ cases and is observed in individuals with genotype MV at codon 129 of the PrP gene and carry PrP^{Sc} Type 2. The mean age onset of disease is about 64 years old and the duration of illness is about 17 months after onset (Parchi, Giese, et al. 1999; Krasnianski et al. 2006).

The phenotype associated with this subtype is characterized by ataxia in almost all patients in the initial state of disease. Cognitive decline is also common. Through the course of the illness, all patients have cognitive decline and ataxia. The patients occasionally feature Parkinsonism, myoclonus and psychiatric signs (Araújo 2013; Gambetti et al. 2003; Puoti et al. 2012).

The patients with sCJD MV2 phenotype have presence of 14-3-3 protein and Tau in the CSF. The MRI is abnormal in all patients (Puoti et al. 2012).

3 Prion disease and PrP^C Cellular trafficking

3.1 Vesicular trafficking

Eukaryotic cells require transport of lipids and proteins between extracellular and intracellular environments and transport of nutrients between organelles also occurs. This transport is accomplished by vesicle formation which bud from a donor compartment and merge with an acceptor compartment in the secretory and endocytic pathways (Chavrier et al. 1990). Coat proteins such as COPI, COPII and clathrin are necessary for membrane deformation on a specific donor compartment. Wherein, the coat protein COPII is necessary for formation of buds from the endoplasmic reticulum to the golgi apparatus. The coat protein COPI is necessary for formation of buds from *cis*-golgi for retrograde transport back to ER and the clathrin is necessary for formation of buds from plasma membrane and *trans*-Golgi network to the late endosomes (Figure 5) (Lodish et al. 2000b).

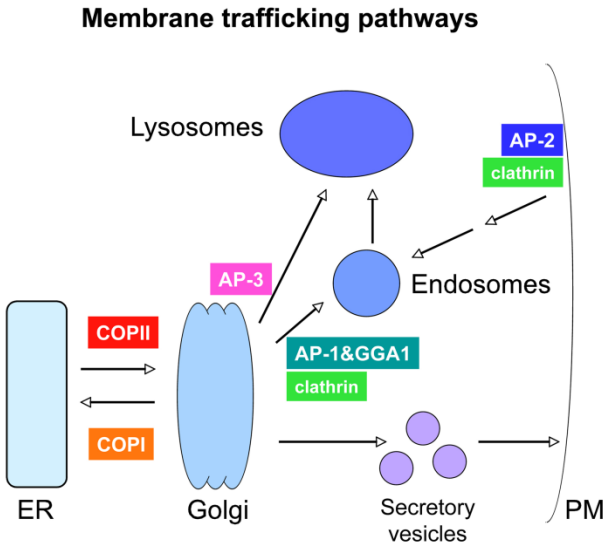

Figure 5. General model of vesicular transport pathways: Transport between organelles is mediated by vesicles. Vesicle formation at various steps is driven by specific coat protein complexes (Take from Grant e Sato, 2006).

The binding of coat proteins to the membrane is regulated by small GTP-binding proteins called ADP-ribosylation factor (ARF) when is associated with COPI-coated vesicles and clathrin-coated vesicles. However, the small GTP-

binding proteins called Sar1 are associated with COPII-coated vesicles. The small GTP-binding proteins bind to membrane receptors. Only and when coat proteins are in the GTP-form they may lead to vesicle budding. Then the complexes of ARF-GTP/Sar1-GTP in the vesicle are hydrolyzed, leading to the conversion of ARF-GDP/Sar1-GDP form and the dissociation of coat proteins from the vesicle membrane (Figure 6). The non-coated vesicles are now a target for SNARES proteins. There are SNARES proteins that bind to non-coated vesicles called v-SNARES, and other that bind to target membrane called t-SNARES. The v-SNARES on the non-coated vesicle bind to the t-SNARES on the target membrane with the aid of Rab proteins, leading to membrane fusion (Gahan 2005).

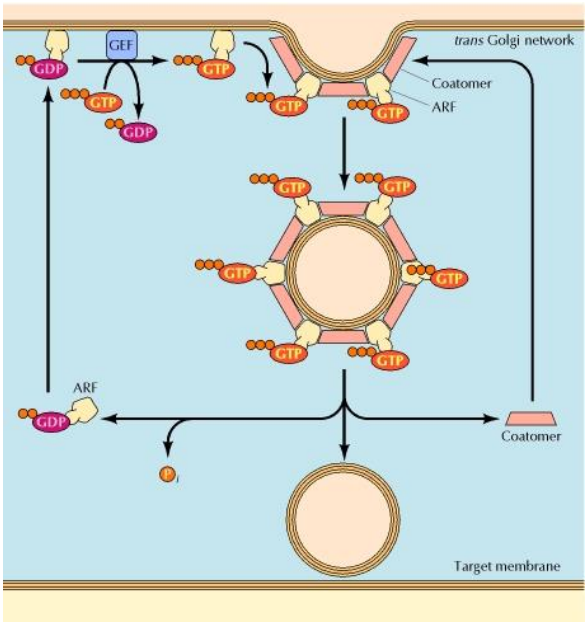

Figure 6. Role of ARF in the formation of COP-coated vesicles: ARF alternates between GTP-bound and GDP-bound states. When bound to GDP, ARF associates with the membrane of *trans* Golgi network, where guanine nucleotide exchange factors (GEF) promote the exchange of the bound GDP for GTP. In its GTP-bound state, ARF promotes the binding of COPI coat protein (coatomer), leading to vesicle budding. Hydrolysis of the bound GTP then converts ARF to the GDP-bound state, leading to disassembly of the vesicle coat prior to fusion with the target membrane (Take from Gahan, 2005).

3.2 Rab GTPases proteins

Rab GTPases belong to the largest branch of Ras superfamily of small GTPases that are necessary to regulate formation, transport, tethering and fusion of vesicles,. In Human cells were identified at least 63 different Rab family members and each Rab protein is localized in the membrane of a specific organelle (each organelle has at least one type of Rab protein) or in the cytosol (between 10 to 50% of Rab proteins can be detected in cytosol) (Figure 7) (Hutagalung & Novick 2011; Schimmoller et al. 1998; Zerial & McBride 2001). In cytosol Rab proteins are in an “inactive” form (GDP-bound) and a cytosolic protein called guanine nucleotide dissociation (GDI) bind to the Rab-GDP. Then, a membrane protein called GDI-displacement factor (GDF) displaces Rab from GDI and inserting Rab protein in the appropriate membrane. After insertion of Rab on the specific membrane, a protein called guanine nucleotide exchange factor (GEF) catalyzes the conversion of GDP-bound Rab to GTP-bound (Collins 2003). The Rab-GTP or “active” form is able now to interact with effector proteins located in that organelle and to regulate vesicle events, for instances, selecting the cargo, promoting vesicle movement and verifying the correct site of fusion (Pfeffer 2001). After, a GTPase accelerating protein (GAP) bind to the Rab-GTP form and catalyzes the hydrolysis of GTP-bound to GDP-bound. Thus, the GAP converts Rab back to its inactive form and is able now to interact with GDI that recruit Rab protein to the cytosol. This Rab protein can then undergo another cycle of GDP-GTP (Figure 8). The cycle between an active and an inactive form, GTP-bound and GDP-bound, regulates temporal and spacial membrane transport and the cycle is restricted to the membrane compartments where they are localized (Zerial & McBride 2001). For instance, Rab5 are localized in membrane of early endosomes and mediatefusion of clathrin-coated vesicles to form the early endosome. While Rab7 proteins are localized in the membrane of late endosomes and mediate transport between early to late endosome. The rate of vesicles fusion is controlled by absolute amount of Rab-GTP form. Thus, the cycle of some individual Rab proteins are essential for specific vesicles fusion and their interaction with V-SNARE proteins are critical to define which vesicle will be fuse with target membrane (Figure 9) (Lodish et al. 2008; Hutagalung & Novick 2011).

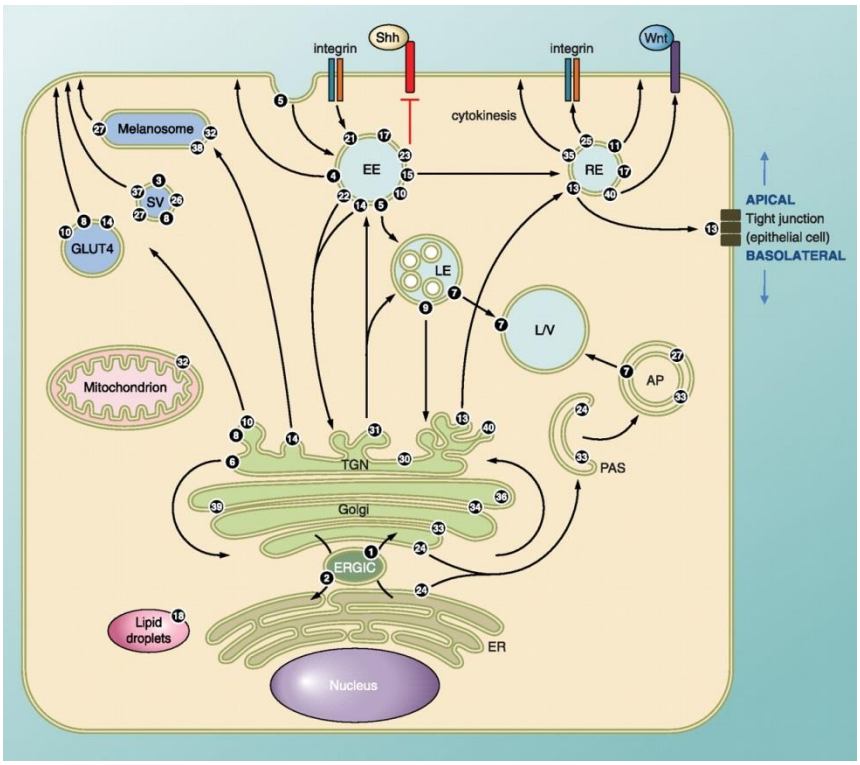

Figure 7. The intracellular localization and associated vesicle transport pathway(s) of several Rab GTPases in eukaryotic cell. Rab1 regulates ER-Golgi traffic while Rab2 is involved in retrograde traffic from Golgi-ER. Rab6 regulates intra-Golgi traffic and several Rabs including Rab8, -10, and -14 regulate biosynthetic traffic from the trans-Golgi network (TGN) to the plasma membrane. Several Rabs are associated with endosomal traffic. Wherein, Rab5 regulated the formation of early endosome. Traffic can be directed towards the lysosome for degradation (regulated by Rab7) or to various recycling compartments to return factors to the plasma membrane (regulated by Rab15). Rab4 and Rab11 regulate fast and slow endocytic recycling, respectively. Specialized Rab functions include Rab18 controls the formation of lipid droplets. Rab33 together with Rab24 regulated the formation of autophagosomes. Rab21 and Rab25 regulate transport of integrins to control cell adhesion and cytokinesis. Rab13 regulates the assembly of tight junctions between epithelial cells. There are several Rabs that they function is poorly characterized or unclear. AP, autophagosome; ERGIC, ER-Golgi intermediate compartment; ER, endoplasmic reticulum; EE, early endosome; LD, lipid droplet; LE, late endosome; L/V, lysosome/vacuole; PAS, preautophagosomal structure; RE, recycling endosome; SV, secretory vesicle/granule (Take from Hutagalung e Novick, 2011).

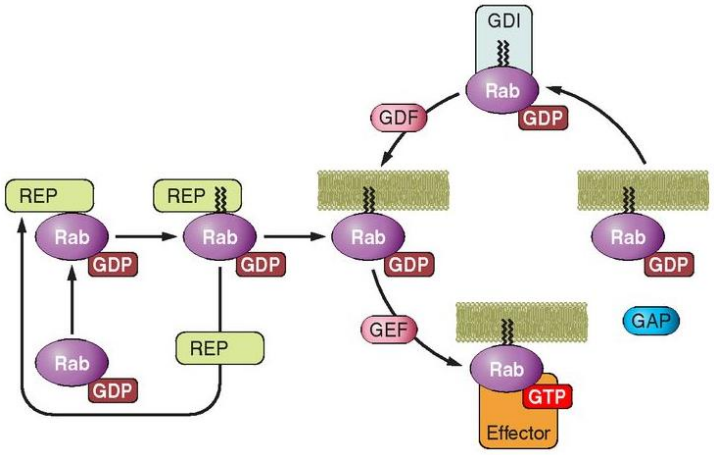

Figure 8. Activation cycle of small G proteins and their regulatory proteins. Rab proteins include COOH-terminal prenylation signals. The Rab escort protein (REP) interacts with newly synthesized Rab and allows the Rab geranylgeranyl transferase (RabGGT) to add two geranylgeranyl lipid groups to the COOH terminus of Rab. Activation of Rab is mediated by a Guanine nucleotide exchange factor (GEF). GTP loading induces the translocation of Rab from the cytosol to the plasmatic membrane and permits the interaction with effectors. To “turn off” the cycle, a GTPase-activating protein (GAP) accelerates the intrinsic GTPase activity of Rab, allowing Rab to return to its inactive state in the cytosol. A guanine nucleotide-dissociation inhibitor (GDI) binds specifically to GDP-bound Rab, prolonging the inactive state and sequestering the GTPase in the cytosol. The insertion of Rab in the target membrane is mediated by a GDI dissociation factor (GDF) that releases the Rab from GDI (Take from Loirand, Sauzeau e Pacaud, 2013).

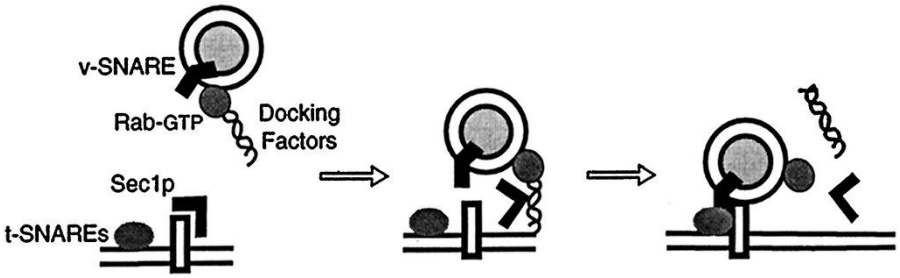

Figure 9. Hypothetical model for Rab-mediated vesicle docking. Transport vesicles carry Rabs in their active, GTP-bound conformations. Active Rabs recruit specific docking factors from the cytosol. We propose that the docking factor·Rab complex can recognize protected t-SNAREs at the target membrane and in some way catalyze t-SNARE deprotection. In this manner, v- and t-SNARE pairing could take place (Take from Schimmoller, Simon e Pfeffer, 1998).

3.2.1 Rab7a protein

The rab7a protein belongs to the Rab family that regulates endosomal traffic. This protein is localized on the surface membrane of late endosomes and lysosomes, thus rab7a regulates the endosomal traffic between early endosome to the late endosome and late endosome to the lysosome (Bucci et al. 2000; Wu et al. 2005). This traffic is regulated by interaction of rab7a with various effectors such as Vps34/p150 PI3-Kinase complex, Rab interacting lysosomal protein (RILP), Rabring7 and proteasome (Dong et al. 2004; Mizuno et al. 2003; Stein et al. 2003). The interaction between Rab7a and a specific effector regulates a specific step. For instance, Rab7a GTP-bound form interacts with RILP protein to regulate the late endosome motility on microtubules to the lysosome (Cantalupo et al. 2001; Jordens et al. 2001). While, the interaction of Rab7a GTP-bound with hVPS34 via the p150 adapter protein activate PI3P formation, together, they regulate internal vesicle formation within multivesicular endosomes (late endosome) and the transport of epidermal growth factor receptor (EGFR) into intraluminal vesicles of MVB (Futter et al. 2001). However, the transport of EGFR into intraluminal vesicles is also regulated by recruitment of alpha subunit XAPC7 of 26S proteasome by Rab7a protein. Studies have shown that recruitment of XAPC7 is critical for the transport of cargo to the late endosome (such as the EGFR) and also its subsequent degradation (Mukherjee et al. 2005; Zafar et al. 2011; Dong et al. 2004).

3.2.2 Rab9 protein

The rab9 proteins are localized on the surface of late endosome and *trans*-Golgi network. Thus, Rab9 regulates endosomal traffic between late endosome and *trans*-Golgi network, retrograde transport. This traffic is regulated by interaction with several effectors such as TIP47, INPP5B, GCC185, PI3P PIKyve Kinase associated protein p40, *Nde*I, 14-3-3 protein theta and HPS4 (Hutagalung & Novick 2011). The interaction between Rab9 and a specific effector regulates a specific step. For instance, the Rab9 protein GTP-bound form interacts with TIP47 to recycling mannose-6-phosphate (MPRs) from late endosome to the *trans* Golgi network (Lombardi et al. 1993).

Studies have shown the impairment of Rab9 effect on late endosomal trafficking to trans Golgi network (Hanna et al. 2002).

4 Microtubules and Tau protein

The cytoskeleton is one of several elements that characterize the eukaryotic cell and consist in a network of fibrous elements. There are three types of fibrous elements, microtubules (MTs), microfilaments (MFs) and neurofilaments (NFs) that are found in the cytoplasm (Figure 10). The microtubules are responsible for the shape of the cell and by transport of vesicles inside the cell. They are constituted by heterodimers of α- and β-tubulin that align to form a hollow tube with an outer diameter of 25 nm. Proteins that bind along the sides of microtubules are collectively called microtubule-associated proteins, or MAPs. MAPs can stabilize microtubules against disassembly. Tau, which is much smaller than most other MAPs, is present in both axons and dendrites (Lodish et al. 2000a).

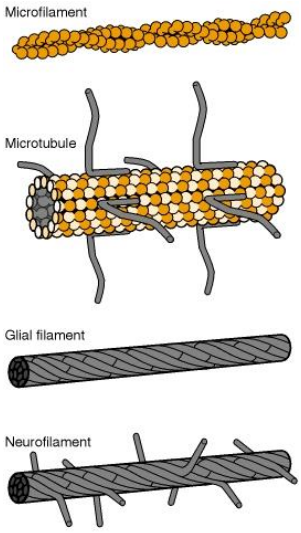

Figure 10. Microfilaments, microtubules and intermediate filaments in the nervous system. Each cytoskeletal structure has a distinctive ultrastructure. This schematic illustrates the major features of the core fibrils. The microfilament consists of two strands of actin subunits twisted around each other like strings of pearls. The individual subunits are asymmetrical, globular proteins that give the microfilament its polarity. The microtubule is also made from globular subunits, but in this case the basic building block is a heterodimer of α- and β-tubulins. These αβ dimers are organized into linear strands, or protofilaments, with β-tubulin subunits oriented toward the plus end of the microtubule. Protofilaments form sheets *in vitro* that roll up into a cylinder with 13 protofilaments forming the wall of the microtubule. Assembly of both microfilaments and

microtubules is coupled to slow nucleotide hydrolysis, ATP for microfilaments and GTP for microtubules. The subunits of both glial filaments and neurofilaments are rod-shaped molecules that will self-assemble without nucleotides. The core filament structure is thought to be a ropelike arrangement of individual subunits. Glial filaments are typical type III intermediate filaments in that they form homopolymers without side arms. In contrast, neurofilaments are heteropolymers formed from three subunits, NFH, NFM and NFL for the high-, medium- and low-molecular-weight subunits. The NFH and NFM subunits have extended carboxy-terminal tails that project from the sides of the core filament and may be heavily phosphorylated (Take from Kirkpatrick e Brady, 1999).

Tau is a protein whose most important function is to stabilize microtubules. These proteins are found mostly in neuronal cells when compared to non-neuronal cells. They are localized along the axon and they stabilize the axonal microtubules and provide flexibility. The ability of Tau to cross-link microtubules into thick bundles may contribute to the stability of axonal microtubules (Lodish et al. 2000a). Tau has 6 different isoforms derived from alternative splicing of a Tau mRNA (Kirkpatrick & Brady 1999). Three isoforms have three binding domains and the other three have four. The binding domains are located in the carboxyl-terminus of the protein and are positively charged (allowing it to bind to the negatively charged microtubule). The isoforms with four binding domains are better stabilizers of microtubules than those with three binding domains. Phosphorylation Tau isoforms regulate the assembly and disassembly of microtubules. For instance, in AD Tau isolated from brain tissue is about 4 times more phosphorylated than in normal brains (Kopke et al. 1993; Ksiezak-Reding et al. 1992).

II. The Aims of the present study

The aims of the present study were undertaken to identify proteins interacting with PrP^C that could provide new insights its physiological functions and pathological role. And also the role of interacting partners of PrP^C, Rab7a and Rab9, in MM1 and VV2 subtype of CJD.

In the present project, the Identification of interacting partners of PrP^C shall be defined by co-localization of PrP^C with Rab7a and Rab9 in neuronal cell models and also in cortex, cerebellum and hippocampus of mice brain wild type (WT). The Identification of Intracellular levels of Rab7a and Rab9 in sCJD-MM1 and sCJD-VV2 shall be analysed in frontal cortex and cerebellum of human brain with sCJD-MM1 and sCJD-VV2 in comparison to the control group consisting of frontal cortex and cerebellum of human brain without neurodegenerative diseases.

In addition, analyse the intracellular levels of Rab7a and Rab9 in pre-symptomatic and symptomatic stages of sCJD-MM1 shall be analysed in cortex and cerebellum from mice with sCJD-MM1, to investigate the intracellular levels of endosomal proteins during diseases progression.

III. Materials

1 Antibodies

Antibodies used for immunoblotting (IB) and immunofluorescence (IF) are listed in Table 2.

Table 2 List of antibodies and their application in present study

Primary Antibody	Origin	Dilution IB	Dilution IF	Company/ Cat. No.
Rab7(D95F2)	rabbit IgG	1:1000	1:50	Cell Signaling/9367
Rab9(D52G8)	rabbit IgG	1:1000	1:50	Cell Signaling/5118
GAPDH	rabbit IgG	1:1000	-	mAbcam 9484
3F4 PrP	mouse IgG2a	1:1000	1:200	Chemicon/MAB1562
Tau	rabbit IgG	1:1000	1:50	mAbcam 64193

Secondary antibody	Origin	Dilution IB	Dilution IF	Company/ Cat. No.
α-mouse-Cy3	goat	-	1:200	Dianova/115-165-146
α-mouse-A488	goat	-	1:200	Invitrogen/522263
α-rabbit-A488	goat	-	1:200	Molecular Probes/A11070

2 Antibiotics

Table 3 List of antibiotics

Antibiotics	Company
Penicillin	Gibco

Streptomycin	Gibco

3 culture media

Table 4 List of culture media

Culture media	Company
Agarose	Biozym
DMEM	Sigma-Aldrich

4 Chemicals

All chemicals used in this study were obtained from Amersham (Freiburg, Germany), Sigma and Fluka (Deisenhofen, Germany), Merck (Haar, Germany), Applichem (Darmstadt, Germany), Serva (Heidelberg, Germany), Roth (Karlsruhe, Germany) and BioRad (München, Germany).

5 Instruments and other materials

Table 5 List of the instruments used in this study

Appliance	Model or Description	Manufacture
Bio-safety Cabinet	Hera safe KS	Heraeus/ Osterode, Germany
Centrifuge	5415C	Eppendorf/Hamburg,Germany
Centrifuge	Rotina 35R	Hettich/ Tuttlingen, Germany
Chamber slide	Lab-Tek™ II Chamber Slide, 15453	nunc/ New York, USA
Culture dishes	60 mm, 351016	Becton Dickinson /NJ, USA
Electro blotting apparatus	Mini Trans-Blot®	Bio-Rad /Munich, Germany
Electrophoresis apparatus	Mini-Protean® III	Bio-Rad /Munich, Germany
Electroporation cuvette	1mm, 748 011	Biozym/ Oldendorf, Germany

Freeze drier	Alpha 1-4 LD	SciQuip Ltd/ Shropshire, UK
Heated magnetic stirrer	iKAMAG RCT	IKA-Labortechnik/ Staufen, Germany
Ice machine	-	Ziegra /Isernhagen, Germany
Incubator	IFE 400	Memmert/ Schwabach, Germany
Microscope	Zeiss LSM 510 Meta	Carl Zeiss/ Goettingen, Germany
Power supply	Power Pac 300	Bio-Rad /Munich, Germany
Safe-Lock tubes	0.2, 0.5, 1.5 and 2ml	Eppendorf /Hamburg, Germany
Semi-Dry transfer Cell	Transblot SD	Bio-Rad/ Munchen, Germany
Serological pipettes	2, 5, 10, 25ml	Sarstedt /Germany
plastic tubes	15 and 50ml	Sarstedt /Germany
pH meter	pH 526	WTW**/** Weilheim, Germany
Shakers	CERTOMAT R	Sartorius/ Goettingen, Germany
Spectrophotometers	EL808	Bioteck instruments/Winooski-vermont, USA
Sterile filter Nalgene	0.2µm	Sartorius/ Goettingen, Germany
Sterile filter pipette tips	-	Biozym /Oldendorf, Germany
Thermomixer	5436	Eppendorf/ Hamburg, German
Vortexer	Genie 2™	Bender and Hobein /Zurich, Switzerland
Water bath	1003	GFL/ Burgwedel, Germany

6 Kits

All the listed kits were used according to the manufacturer's instructions.

Table 6 list of the kits used in this study

Name	Company/ Cat. No.	Application
Caspase-3 activity assay kit	Promega/G7220	Apoptotic activity assay
Lipofectamine 2000	Invitrogen	Liposome-mediated transfection

7 siRNA Duplex

Table 7 List of siRNA Duplex

siRNA Duplex	Sequence (5'-3')	Accession/Cat. No.
siRNA-Rab7a	CUGCUGCGUUCUCCUAUUU	Operon
siRNA Negative control	-	EUROGENTES/SR-CL000-005
siRNA-Tau	CGUACACUGAGUUCGAGCU	Operon
siRNA Negative control	-	EUROGENTES/SR-CL000-005

8 Software

The list of scientific software used in the study is in table 8.

Table 8 List of scientific software

Program	Use	References
Graphpad Prism 5	Statistical analysis	GraphPad Software, Inc.

		California, USA
ImageJ 1.43u	Densitomatric analysis	National institutes of Health, USA
ImageJ 1.43u WCIF	Colocalization analysis	National institutes of Health, USA
KC4 V3.4	Absorbance reader	Bioteck instruments, USA
LabImage 2.7.1	Densitomatric analysis	Kapelan GmbH, Halle, Germany
Protein-Lynx-Global-Server v 2.1	LS MS/MS data analyzer	Micromass, Manchester, U.K
Zeiss LSM 4.2.0.121	Immunofluorescence	MicroImaging GmbH, Goettingen, Germany

9 Stock solutions

Blocking solution for WB: 5% Milk Powder in TBS-T.

Cell lysis buffer I: 50 mM Tris-HCl pH 8.0, 0.5% CHAPS, 1mM EDTA, 1% triton x100.

Cell lysis buffer II: 7 M urea, 2 M thiourea, 4% CHAPS, 2% ampholytes, 1% DTT and a protease inhibitor mixture.

Electrophoresis buffer (SDS-running buffer): 192 mM glycine, 0.1% SDS, 25 mM Tris-HCl pH 8.3.

TBE: 42 mM Boric Acid, 10 mM EDTA, 50 mM Tris-HCl pH 8.0.

TBS-T: TBS and 0.1% of Tween-20.

TE: 0.01 M Tris-HCl, pH 7.4, 1 mM EDTA pH 8.0

Transblot buffer for PVDF membrane (semi dry): 192 mM Glycine, 10% methanol, 25 mM Tris-HCl pH 8.3.

IV Methods

1 Biological samples

1.1 Human brain

Frontal cortex and cerebellum samples from 30 pathologically confirmed sCJD patients (15 of each MM1 and VV2 subtypes) and 15 age-matched control cases (CON) were used in this study. All 45 samples were obtained from the Institute of Neuropathology Brain Bank (HUB-ICO-IDIBELL Biobank) and Biobank of Hospital Clinic-IDIBAPS. The mean age and gender of study cases were as described previously (Llorens et al. 2013). In brief, for sCJD western blot analysis in frontal cortex: 60 years of age in control (10M/5F), 68 sCJD MM1 (10M/5F), 63 sCJD VV2 (5M/10F). In cerebellum, the mean age was 62 in control (11M/4F), 66 sCJD MM1 (10M/5F) and 63 in sCJD VV2 (4M/10F). After post-mortem interval ranging 1h 45min. to 24h 30min., coronal sections 1cm thick were cut from one of the hemispheres. Along with selectively dissected areas of encephalon, coronal sections were rapidly frozen on metal plates over dry ice, sorted in separate bags, labeled with water-resistant ink and stored at -80^{o}C until further use for biochemical investigations. The other hemisphere was was immersed fixed in 4% buffered formalin for 3 weeks for morphological studies and neuropathological examination and characterization. The analysis of the codon 129 genotype of PrP gene (Met: M or Val: V) was performed after isolation of genomic DNA from blood samples according to standard methods. Western blot profile of PrP^{Sc} was classified as type 1 or type 2 based on electrophoretic mobility after proteinase K (PK) digestion.

1.2 sCJD MM1 mice brain

Double transgenic mice overexpressing about 4-fold level of human PrP^{C} with methionine at codon 129 (Met129) on a murine PrP knock-out background were used, as described previously (Padilla et al. 2011). Inocula were prepared from sCJD MM1 brain tissues as 10% (w/v) homogenates. Individually identified 6-10 week-old mice were anaesthetised and inoculated with 2 mg of brain homogenate in the right parietal lobe using a 25-gauge disposable hypodermic needle (6 animals per group and time point). Mice were observed daily and the

neurological status was assessed weekly. When disease progression was evident, or at the end of lifespan, animals were euthanized, necropsy was performed, and the brain was removed. A part of the brain was fixed by immersion in 10% buffered formalin to quantify spongiform degeneration and perform immunohistological procedures. The other part was frozen at −80°C to extract protein. Survival time was calculated for each isolate and expressed as the mean of the survival day post-inoculation (DPI) of all mice scoring positive for PrP^{Sc}. Infection rate was determined as the proportion of mice scoring positive for PrP^{Sc} from all inoculated mice.

2 Immunoblot

Tissue lysis and immunoblotting were performed as described previously [Zafar et al., 2014]. Briefly, cells were lysed (50mM Tris-HCl, pH8, 1% Triton X-100, 0.5% CHAPS, 1mM DTT), and lysates were cleared of cell debris (1 min., 1000 xg, 4°C). Cell lysates were supplemented with protease and phosphatase inhibitors (Roche) and were separated on 12.5% 1-DE SDS-PAGE. The proteins from SDS-PAGE were transferred to a PVDF blotting membrane and were incubated with antibodies against Rab7a and Rab9 (D95F2 and D52G8, 1:1000, Cell Signalling). The primary antibody was detected by incubation of secondary antibodies of anti-rabbit in 5% milk (1:5000)**.** Membranes were then rinsed in 1x TBS-T and incubated with the corresponding horseradish peroxidase-conjugated secondary antibody (diluted 1:2000/1:5000) for 1h at RT. Immunoreactivity was detected after immersion of the membranes into enhanced chemiluminescence (ECL) solution and exposure to ECL-Hyperfilm (Amersham Biosciences, Buckinghamshire, UK). Images were documented using the ScanMaker4 (Microtek, International), after correction for the background, and band intensities were determined by densitometry using Labimage (version 2.7.1, Kapelan GmbH, Germany) data analyzer software.

3 Immunofluorescence

Frozen cortex, cerebellum and hippocampus of wild type mice (see section III, 1.2) were embedded in cryomatrix and 5 µm thick sections were sliced using

cryostat (Leica cryostat 3050). These sections were mounted on histological glass slides, fixed in acetone for 1 minute, washed with methanol for 10 minutes and air dried. After, slides were hydrated in PBS for 10 minutes and incubated overnight with primary antibodies (anti-PrPc 3F4 (1:200) and rabbit anti-Rab7a (1:50)) diluted in PBS supplemented with 0.2% TritonX-100 at 4ºC overnight. After incubated overnight, we washed 3 times for 5 min. with PBS and incubated with secondary antibody for 1h at room temperature. The slides were washed with PBS (3x, 5 min.) and mounted with cover slip using anti fade mounting medium. Slides were visualized using a confocal laser scanning microscope.

4 Primary culture of mouse cortex

The wild type pregnant mice at embryonic day 14 under halothane (Sigma) anesthesia were sacrificed by cervical dislocation. The embryonic cerebral cortex were isolated and dissociated by mechanically dissociated and plated on polyethylenimine (1 mg/ml)-coated glass cover-slips in culture wells. For the brefeldin-A (BFA, Cell Signalling) treatment, cell cultures were first grown in Dulbecco's Modified Eagle's Medium (DMEM, Sigma-Aldrich), supplemented with 5% fetal bovine serum (FBS, Biochrom AG), 2.5% fetal calf serum (FCS, Eurobio), 2 mM glutamine, and 0.1% penicillin and streptomycin (Gibco), at a density of $7x10^5$ cell/cm^2. After 3 days in vitro (DIV), the medium was replaced with N5 medium [Kawamoto & Barrett, 1986] with 180 mg/L glucose and supplemented with 5% FBS and 1% FCS. Then 3 μM cytosine arabinoside (Sigma, St Louis, MO, USA) was added to prevent astrocyte proliferation (resulting in at least 97% pure neuronal culture), and 1 μM MK-801 (Research Biochemicals International) to present excitotoxicity (Knusel et al. 1990). The medium was changed daily. On DIV 5, FCS was removed and the FBS content was reduced to 1%. Cells were cultured at 37C in humidified 5% CO_2 atmosphere.

5 Liposome-mediated transient transfection

Transfection assay were performed using LIpofectamine 2000 (invitrogen) according to the manufacturer’s instructions. The primary culture of mice cortex (see section III, 4) were plated in 6-well plates at a cell density of 2-5 x 10^5 per well

and maintained for 24h in the medium containing 10% FBS (about 70-90% confluent). After cell culture reaching approximately 70% confluency, 4 µg of each plasmid and 10µL of Lipofectamine 2000 were incubated separately in 250 µL of Opti-MEM I Reduced Serum Medium (Invitrogen). After 5 min. of incubation at room temperature, the diluted plasmids and Lipofectamine 2000 were combined and incubated for an additional 20 minutes at room temperature. The DNA-Lipofectamine 2000 complexes (5µg) were then added to each well, and the cells were incubated for 24h at 37°C in a CO_2 incubator. After incubation, the transfection medium was replaced with DMEM supplemented complete medium. Cells were collected from confluent cultures after 48h of transfection.

Small interfering RNA (siRNA) transfections were performed with 100nM siRNA using Lipofectamine 2000 (Invitrogen, Carlsbad, CA, USA) according to the manufacturer´s instructions. Rab7a siRNA duplex was a targeted with the sequence 5'-CUGCUGCGUUCUCCUAUUU-3' and Tau siRNA with the sequence 5'-CGUACACUGAGUUCGAGCU-3'. The cells were also simultaneously transfected with Non-targeting siRNA duplex (control siRNA duplex negative control: Eurogentec) was used as a negative control. Transfected cells were cultured for 48h and were lysed (see section III, 6) for expression analysis and immunofluorescence (see section III, 3) for localization studies.

6 Cell lysis

After transfection of primary cell culture, the cells were washed with ice cold 1xPBS, scraped and centrifuged at 4ºC for 5 minutes at 400xg. The pallet was resuspended in ice cold 1x PBS and centrifuged at 4ºC for 5 min at 400xg. The washed cells were lysed in lysis buffer (50 mM Tris-HCL, pH 8, 1% Triton X-100, 0.5% CHAPS, 1mM DTT, protease and phosphatase inhibitor cocktail). Cells lysates were homogenized with ultra sonicator on ice and the lysates were centrifuged for 15 min. with 543,000xg at 4ºC. Protein concentration was estimated by Bradford essay (see section III, 7).

7 Protein concentration estimated by Bradford assay

The protein concentration was estimated by Bradford essay (Bio-Rad). Bradford reagent was prepared by diluting a 1x dye reagent (Bio-Rad) with dH_2O (1:5). To standard curve, we used different dilution of BSA in ddH_2O (1000µg/L; 750µg/L; 500µg/L; 250µg/L; 100µg/L and 50µg/L) in a total volume of 20µg. Protein samples of unknown concentration were diluted in ddH_2O (1:19). Protein standards (to standard curve) and protein samples of unknown concentration were mixed with 980µl of Bradford reagent and incubated for 10 min. at room temperature. The absorbance of the samples was measured at 595 nm. The calculation of the protein concentration was done using Microsoft Office 2007 Excel software.

8 Immunofluorescence and quantification analysis

Primary cells culture (see section III, 4) and primary cell culture transfected with siRNA (see section III, 5) were plated on chambered slides (Lab-TEK II; Thermo Fisher Scientific (Nunc GmbH and Co. KG), Langenselbold Site) and fixed for 5 min. with 100% ethanol. After, the cells were permeabilised with 0.2% Triton X-100 in 1xPBS for 20 minutes. Colocalization of PrP^c with Rab7a and Rab9 was detected by applying the primary antibodies (anti-PrP^c 3F4 (1:200), rabbit anti-Rab7a (1:50) and rabbit anti-Rab9 (1:50)) for overnight at 4ºC. To Colocalization of Total-Tau with Rab7a was also detected by applying the primary antibodies (anti-Tau (1:200) and rabbit anti-Rab7a (1:50)) for over-night at 4ºC. The primary antibodies were detected by incubation the slides for 60 min. with secondary antibodies (Alexa 488 conjugated anti-rabbit (1:200) and Cy3-labeled anti-mouse secondary antibody (1:200)). Incubation with Hoechst 33342 or with TOPRO-3 iodide for 10 min. was performed to visualize nucleosomes. Finally, cover slips were placed on glass slides and mounted with Fluoromount (DAKO, Hamburg, Germany). After secondary antibody incubation all the steps were carried out in a dark humid chamber. The slides were kept dry dark at 4ºC until further microscopic evaluation.

We performed confocal laser scanning microscopy using a LSM 510 laser-scanning microscope (Zeiss, Göttingen, Germany; 488 nm Argon, 543 and 633 nm

Helium-Neon excitation wavelengths) according to the manufacturer´s instructions. Individual images of PrP^c, Rab7a, Rab9 and Tau were analyzed separately by ImageJ (WCIF plugin) software. For two-color analysis, stacks of images with a total thickness of approximately 30µm were acquired, using a dynamic range of 12 bits per pixel. Co-localization expressed as a correlation coefficient indicates the strength and direction of linear relationship between two fluorescence channels. Pearson's linear correlation coefficient (r_p) was used in this study to calculate fluorescence channel correlation (Manders et al. 1992):

$$r_p = \frac{\sum_i (R_i - R_{aver}) \cdot (G_i - G_{aver})}{\sqrt{\left[\sum_i (R_i - R_{aver})^2 \cdot \sum_i (G_i - G_{aver})^2\right]}},$$

Where R_i and G_i are the red and green intensity measures, respectively.
R_{aver} and G_{aver} are the average values of Ri and Gi, respectively.

The r_p values can range from -1 to 1. An r_p of -1 indicates a perfect negative linear between variables, an r_p of 0 indicates no linear relationship between variables, an r_p of >0 indicate a positive correlation and an r_p of 1 indicates a perfect positive linear relationship between variables. The values close to zero of the correlation coefficient are difficult to interpret when the degree of overlap is the quantity to be measure. Wherein, colocalization in the context of fluorescence microscopy were calculated according to published methodology (Manders et al. 1993):

$$M_1 = \frac{\sum_i R_{i,coloc}}{\sum_i R_i},$$

And

$$M_2 = \frac{\sum_i G_{i,\text{coloc}}}{\sum_i G_i},$$

Where $R_{i,coloc} = R_i$ if $G_i > 0$ and $R_{i,coloc} = 0$ if $G_i = 0$, and where $G_{i,coloc} = G_i$ if $R_i > 0$ and $G_{i,coloc} = 0$ if $R_i = 0$. The values of these coefficients, M1 and M2, ranges from 0 to 1. A value of 0 indicates that none of the signal within thresholds in that channel exists as co-localized with the other channel. A value of 1 indicates that the entire signal within thresholds in that channel exists as colocalized with the other channel. Two perfectly colocalized images will generate a scatter plot where the points fall in a line at 45° to either axis.

9 Statistical analysis

The statistical significance of the difference between control and sCJD VV1 and VV2 as also between control and siRNA in western blot was determined by student´s t-tests (GraphPad Prism 5 software). Pvalue less than 0.05 was considered statistically significant. To statistical significance of co-localization of PrP^c and Rab7a and Rab9 in cell culture was determined by Pearson's correlation and M1 and M2 coefficients (Imagej (WCIF plugin) software.

10 Ethics Statement

Human samples from the Institute of Neuropathology Brain Bank (HUB-ICO-IDIBELL Biobank) and Biobank of Hospital Clinic-IDIBAPS were obtained following the Spanish legislation (Ley de la Investigación Biomédica 2013 and Real DecretoBiobancos, 2014) and the approval of the local ethics committees.

All animal experiments were performed in accordance with the ethical standard set by Regierungspräsidium Tübingen (Regional Council) Experimental No. FLI 231/07 file reference number 35/9185.81-2. All animal experiments have been performed in compliance with the institutional and French national guidelines, in accordance with the European Community Council Directive 86/609/EEC. The experimental protocol was approved by the INRA Toulouse/ENVT ethics committee.

IV Results

1 Intracellular levels of Rab7a and Rab9 proteins in frontal cortex and cerebellum of human brain

To know how endosomal pathway is affected in case of sCJD MM1 and VV2 disease, we analyzed the Rab7a and Rab9 proteins expression in frontal cortex of sCJDMM1 and VV2 patients and in cerebellum of sCJD MM1 and VV2 patients by western blots.

In frontal cortex, we observed a increased intracellular levels of Rab7a and a decreased intracellular levels of Rab9 in sCJD MM1 patients as compared to the control. However, patients with sCJD VV2 didn't have any significance difference. In cerebellum, we observed an up-regulation of Rab7a and a down-regulation of Rab9 in sCJDMM1 and sCJDVV2 patients as compared to the control (Figure 11).

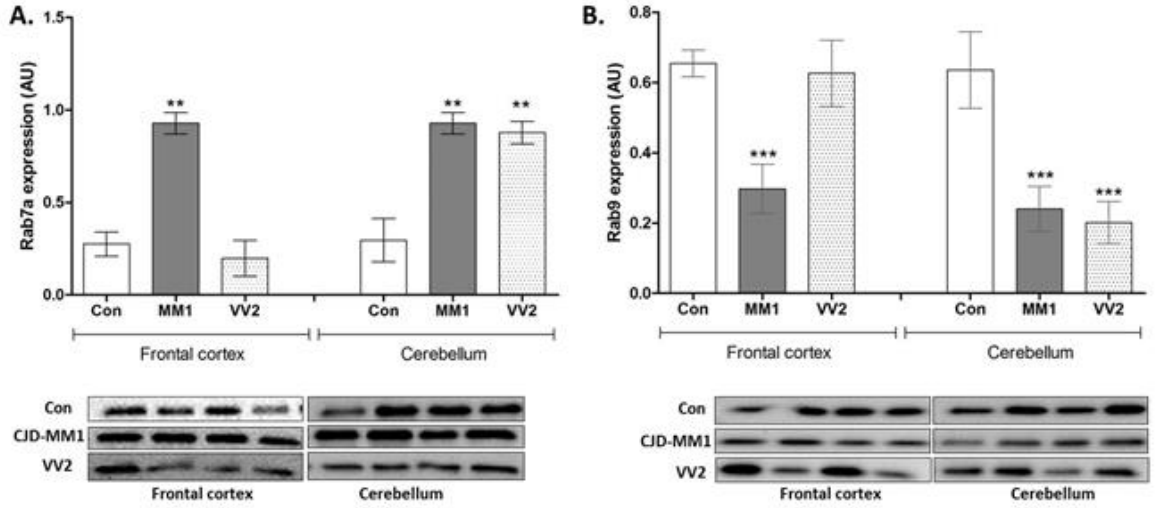

Figure 11. Intracellular levels of Rab7a and Rab9 proteins in frontal cortex and cerebellum human samples of sCJD MM1 and VV2 patients: Western blots of sCJD MM1(n=15), sCJD VV2 (n=15) and control (n=15) was performed separately. To observe the expression of Rab7a and Rab9 primary antibody anti-Rab7a and anti-Rab9 were used and the expression was measured by densitometry. **(A)** The Box Plot from western blot was used to represent the intracellular expression of Rab7 in the frontal cortex and cerebellum of sCJD MM1 and sCJD VV2 compared to the healthy age-matched control. sCJD MM1 and VV2 patients had a significant difference (P value < 0.01 (**) and P value < 0.001 (***)). **(B)** The Box Plot from western blot was used to represent expression of Rab9 protein in the cerebellum of sCJDMM1 and VV2 patients compared to the healthy age-matched control. Both, MM1 and VV2 subtypes of sCJD had a significant difference (P value < 0.001 (***)).

2 Intracellular levels of Rab7a and Rab9 in sCJD-Mice

To analyze the expressional regulation of Rab7a and Rab9 during disease progression, we performed immunoblotting in cortex and cerebellum from the mice with sCJD MM1 at pre-symptomatic and symptomatic stages. In the pre-symptomatic stage, we observed low intracellular levels of Ran9 in the cortex and cerebellum and low intracellular levels of Rab7a in the cortex (figure 12A, B, C). However, we observed a high intracellular level of Rab7a in the cerebellum at pre-symptomatic stage (figure 12B).

In the symptomatic stage, we observed high intracellular levels of Rab9 in the cortex and cerebellum and high intracellular levels of Rab7a in the cortex (figure 12A, B, C). In the cerebellum, we observed low intracellular levels of Rab7a at symptomatic stage (figure 12B).

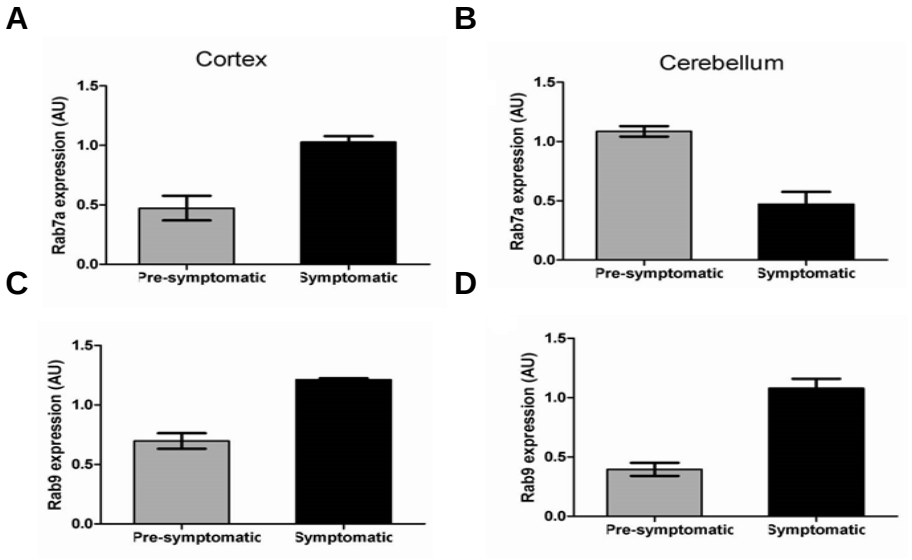

Figure 12. Intracellular levels of Rab7a and Rab9 in sCJD-Mice at pre-symptomatic and symptomatic stages: For characterization of sCJD MM1, all results of the intracellular levels of Rab7a and Rab9 expression from mice´s cortex and cerebellum by western blot were combined and divided in two different stages of disease, pre-symptomatic and symptomatic stages. **(A)** Expression of Rab7a in the cortex, **(B)** Expression of Rab7a in the cerebellum **(C)** Expression of Rab9 in the cortex, **(D)** Expression of Rab9 in the cerebellum.

3 Co-localization of PrP^c and Rab7a by Immunofluorescence

The significant different intracellular levels of Rab7a protein in the brain of sCJD patients, compared to healthy control provided evidence that Rab7a might be an interacting partner of PrP^C. To further check the potential interaction and influence of Rab7a on PrP^C localization and intracellular levels, we performed immunofluorescence of cortex, cerebellum and hippocampus sections from wild type mice to observe the spatial overlap between PrP^C and Rab7a. Therefore, we used two different fluorescent labels with different emission wave length, Cy3-labeled with anti-mouse to observe the localization of PrP^C (red) and Alexa 488 conjugate with anti-rabbit to observe the localization of Rab7a protein (green). Three images were taken for each sections of brain, one with fluorescent red (PrP^C), the second with fluorescent green (Rab7a) and the third merged image where labeled images were combined and overlapping pixels turn yellow. PrP^C showed co-localization with Rab7a in the cytosolic area of cortex, cerebellum and hippocampus. In hippocampus and cortex the co-localization were disperse and in cerebellum it was in a specific region. To determine how much green and red colours overlap, Imagej (WCIF plugin) software was used. Therefore, after merging of PrP^c with Rab7a images, the software generates a scatter plot. A scatter plot is a diagram with green intensities in the X axes and red intensities in the y axes. In the situation of co-localization, the points fall in a line at 45° either axis with yellow intensities. The colour of scatter plot pixel represents the colour of merged image. The scatter plot didn´t show the frequency of the pixels, but is used to show a partial co-localization between PrP^c and Rab7a (Figure 13A).

To quantify co-localization of PrP^C and Rab7a, we used Pearson's correlation coefficient and M1 and M2 coefficients. The values for Pearson's will range from 1 to -1, where values of 1 indicate perfect correlation, 0 indicate random localization and -1 indicate perfect exclusion. Values close to zero and negative for Pearson's correlation coefficient for fluorescent images can be difficult to interpret. However, a value close to 1 does indicate reliable co-localization. The values of M1 and M2 range from 0 to 1, where values of 0 indicate that none of signal within thresholds in that channel colocalizes with the other channel. A value of 1 indicates that the entire signal within thresholds in that channel co-localizes

with the other channel. The Pearson´s correlation and M1 and M2 were used to characterize the degree of overlap between images.

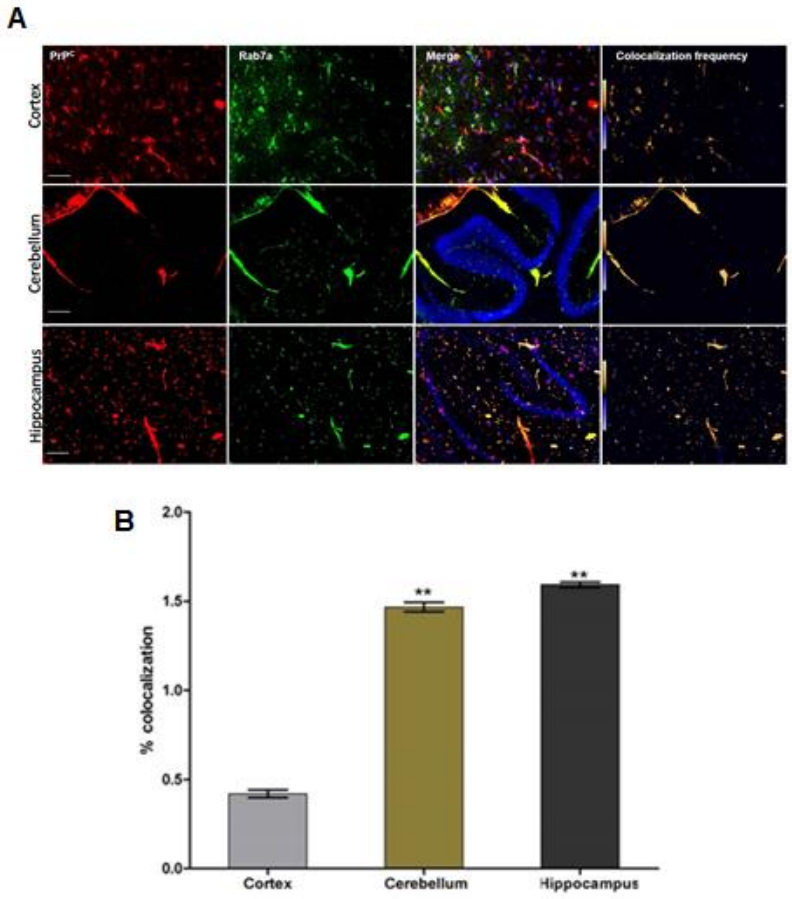

Figure 13. Co-localization of PrPc and Rab7a: (A) PrP^C and Rab7a proteins were analyzed by using 3F4 anti-PrP^C (red), anti-Rab7a (green). **(B)** Statistical analysis (student´s T-test) shown a significant co-localization of PrP^C and Rab7a in the cortex, cerebellum and hippocampus (Pvalue <0,01 (**)) when compared to the cortex.

4 Intracellular levels of PrP^c and Rab7a/Rab9 protein in primary culture of mouse cortex

To further check the potential interaction and influence of Rab7a and Rab9 on PrP^C localization and intracellular levels, we performed the immunofluorescence in primary cells culture of mice´s cortex from wild type mice to observe the spatial overlap between PrP^c and Rab7a/Rab9. To analyze the co-localization between PrP^c and Rab7a/Rab9, we performed two slides with two different fluorescent labels with different emission wavelength. In one of the slides,

we used Cy3-labeled with anti-mouse to observe the localization of PrP^{c} (red) and Alexa 488 conjugate with anti-rabbit to observe the localization of Rab7a protein (green). In the other slide, we used Cy3-labeled with anti-mouse to observe the localization of PrP^{c} (red) and Alexa 488 conjugate with anti-mouse to observe the localization of Rab9 protein (green) (figure 14A). Three images were taken from each slides; one with fluorescent red (PrP^{c}), the second with fluorescent green (Rab7a or Rab9) and the third merged image where the labeled was combined and overlapping pixels turn yellow. PrP^{c} showed co-localization with Rab7a and Rab9 in the cytosolic area, however the percentage of co-localization of PrP^{c} with Rab7a was most significant than PrP^{c} with Rab9 (figure 14B). The scatter plot didn´t show the frequency of the pixels, but is used to show a partial co-localization between PrP^{c} and Rab7a or Rab9 (Figure 14A). The results of Pearson's correlation coefficient of co-localization demonstrated a partial co-localization between Rab7a and PrP^{C} (Figure 14).

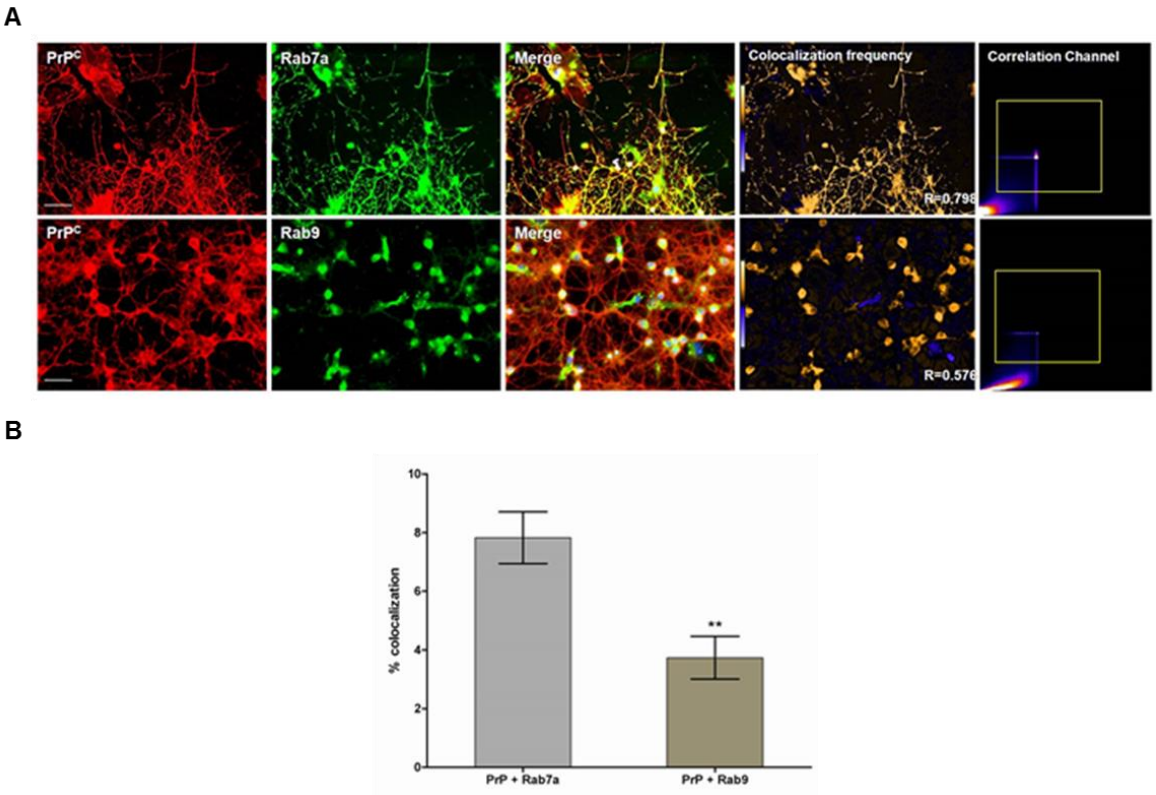

Figure 14. Co-localization of PrPc with Rab7a/Rab9 in primary culture of mouse cortex: (A) PrP^{C}, Rab7a and Rab9 protein was analyzed by using 3F4 anti-PrP^{C} (red), anti-Rab7a (green) antibodies and anti-Rab9 (green). **(B)** Percentage of co-localization of PrP^{C} and Rab7a, and

percentage of co-localization PrP^C and Rab9. The student´s T-test showed less co-localization of PrP^C and Rab9 when compared between PrP^C and Rab7a protein (Pvalue < 0,01 (**)).

PrP^C distribution was then evaluated after depleting Rab7a expression using the siRNA duplex. The localization pattern of PrP^C staining was dramatically altered in primary culture cells treated with siRNA-Rab7a when compared to the primary cells treated similarity but without siRNA (control) (Figure 14A and 15A). We also observed a increased intracellular levels of PrP^C (Figure 15B). However, it was not observed any significant difference in the intracellular levels of Rab9 primary culture cells treated with siRNA-Rab7a (Figure 15C).

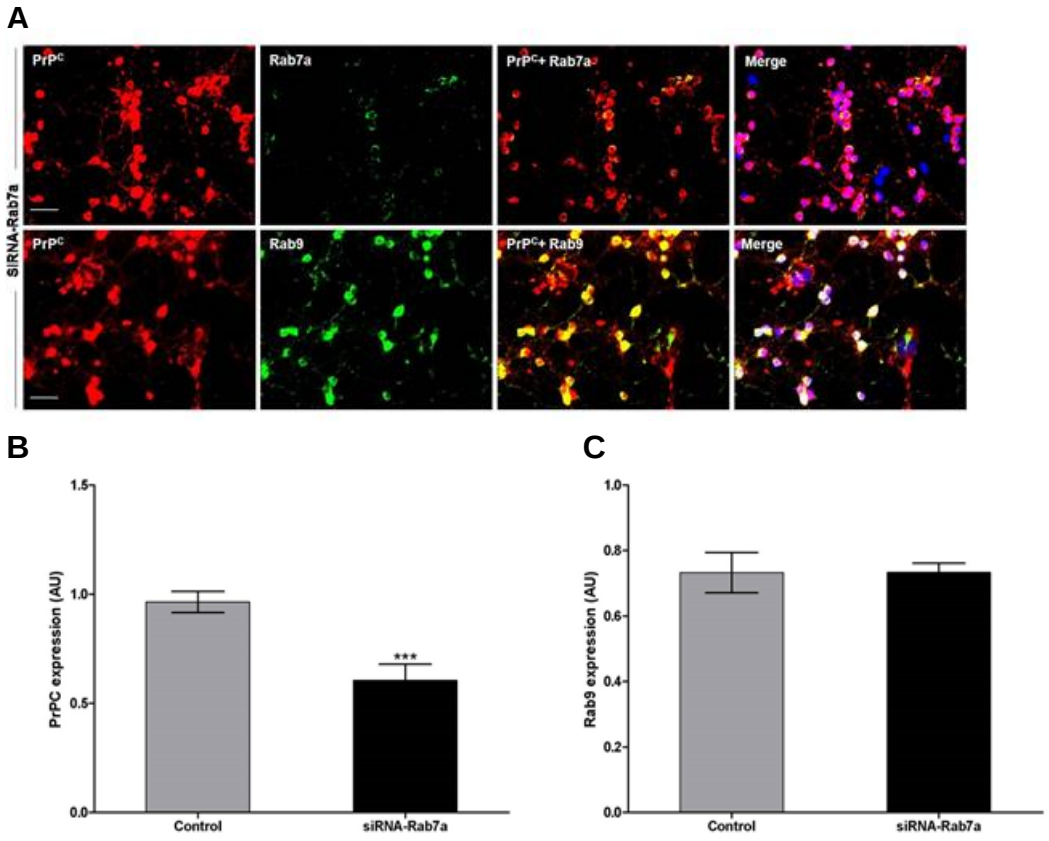

Figure 15. Effect of Rab7a depletion on PrP^C localization: (A) Primary culture cortex mice was treated with siRNA duplex (100 nM) to target Rab7a. Forty-eight hours after transfection, PrP^C, Rab7a and Rab9 intracellular levels was analyzed by using 3F4 anti-PrP^C (red), anti-Rab7a (green) and anti-Rab9 (green) antibodies. The PrP^C is clustered in specific regions of the cytoplasm after treated with siRNA-Rab7a. **(B, C)** Statistical analysis (student´s T-test) show a significant decresed intracellular levels of PrP^C (Pvalue <0,001 (***)) when compared to the control and the intracellular levels of Rab9 did not have any significant difference.

5 siRNA downregulation of Rab7a/Rab9 and Tau

To know if Tau protein affects the intracellular levels of Rab7a and Rab9 proteins, we analyzed the intracellular levels of Rab7a and Rab9 from a cell culture of wild type mice´s cortex treated with siRNA-Tau and without siRNA treated (control) by western blot. After treatment with siRNA-Tau, the expression of Tau protein was inhibited. We observed a significant increased intracellular levels of Rab7a and Rab9 proteins in cell culture treated with siRNA-Tau as compared with control (Figure 16B).

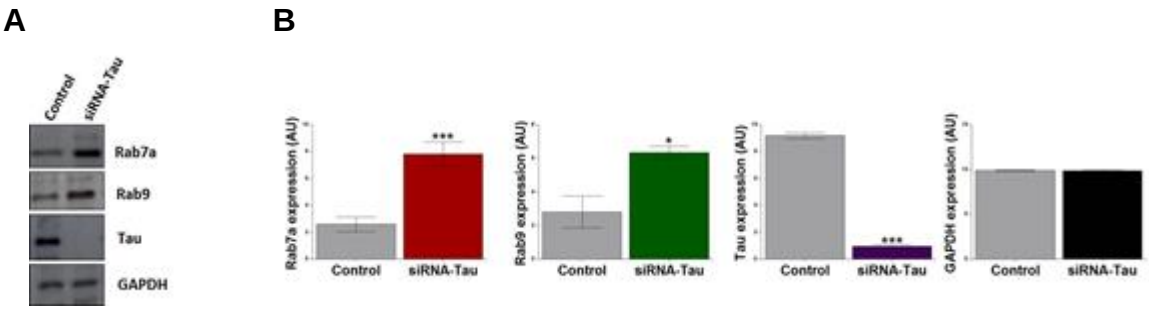

Figure 16. Western blot of primary cortical neurons: (A) Cell culture of wild type mice´s cortex was transfected with siRNA duplex (100nM) to the target Tau. The intracellular levels of Rab7a and Rab9 was analyzed after 48 H of transfection by immunoblotting using specific Rab7a and Rab9 antibodies. **(B)** Densitometry analysis from four independent immunoblotting experiments and significance was calculated by student´s T-test (Pvalue < 0.05 (*), < 0.01 (**), < 0.001 (***)).

6 Tau and Rab7a

Western blot essay in cell cultures with siRNA-Tau provided evidence that Tau might be an interacting partner of Rab7a (figure 16B). To further check the potential interaction and influence of Tau on Rab7a localization and intracellular levels, cell cultures of mice´s cortex from wild type mice were treated with siRNA-Tau, siRNA-Rab7a and Nt-siRNA (control) followed by immunofluorescence. To analyze the co-localization between Tau and Rab7a, we performed three slides with two different fluorescent labels and different emission wavelengths. In each slide we used Cy3-labeled with anti-mouse to observe the localization of Total-Tau (red) and Alexa 488 conjugate with anti-rabbit to observe the localization of Rab7a protein (green) (figure 17A). Three images were taken from each slide; one with

fluorescent red (Total-Tau), the second with fluorescent green (Rab7a) and the third merged image where the labeled images were combined and overlapping pixels turn yellow. Total-Tau showed a co-localization with Rab7a in cytosolic area in cell cultures without siRNA (control) (figure 17C). In cell cultures treated with siRNA-Rab7a, we observed a significant decreased intracellular levels of Total-Tau and their localization was altered as compared with control (figure 17A).

In cell cultures treated with siRNA-Tau, we observed a significant increased intracellular levels of Rab7a and localization of Rab7a was altered as compared to cell cultures without siRNA (control) (figure 17A).

To determine the percentage of overlap, we used Imagej (WCIF plugin) software. To quantify the co-localization of Total-Tau with Rab7a, we used Pearson's correlation and M1/M2 coefficient.

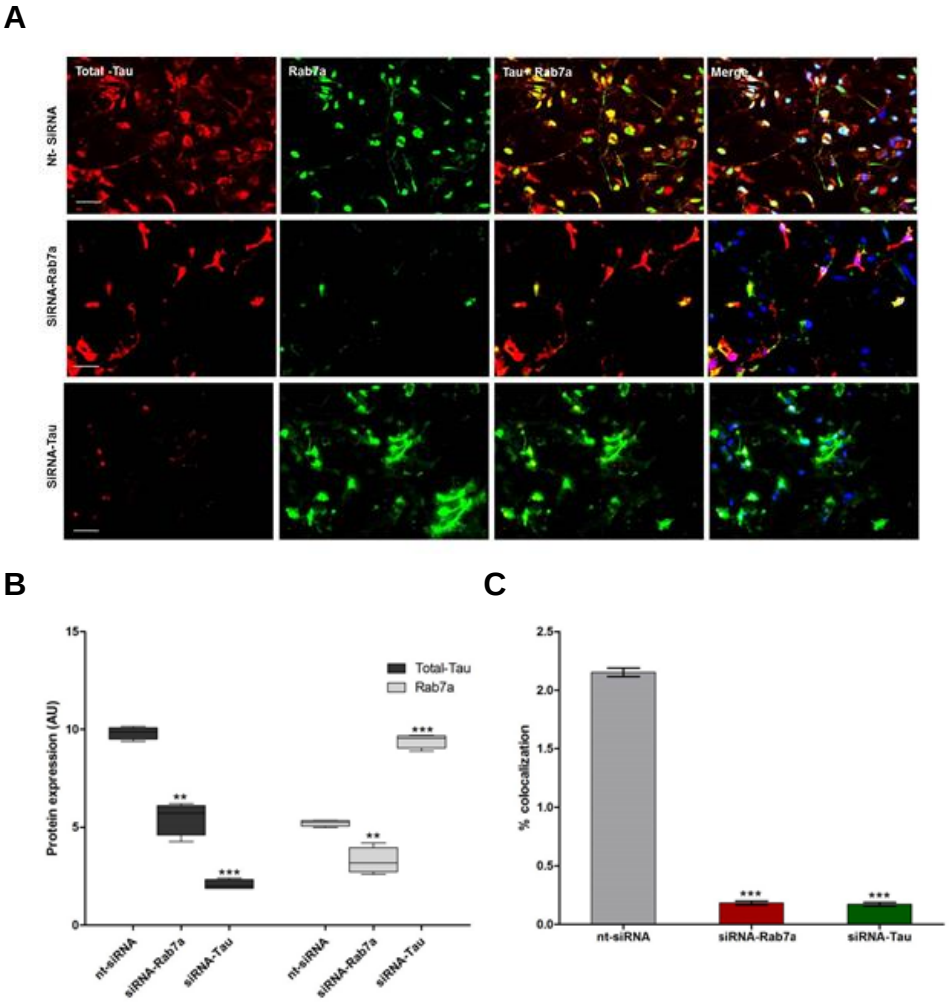

Figure 17. Intracellular levels of Total-Tau and Rab7a in a cortex primary culture of wild type mice treated with siRNA-Rab7a and siRNA-Tau: (A) Primary cultures of mice´s cortex was treated with siRNA duplex (100 nM) to target Rab7a and Tau and without siRNA (control). Forty-eight hours after transfection, Total-Tau and Rab7a expression was analyzed by using anti-Tau (red) and anti-Rab7a (green) antibodies. The Total-Tau is clustered in specific regions of the cytoplasm after treated with siRNA-Rab7a. (B) Statistical analysis (student´s T-test) shown a significant decreased intracellular levels of Total-Tau in cell culture treated with siRNA-Rab7a and an increased intracellular expression of Rab7a in cell culture treated with siRNA-Tau when compared with cell culture without siRNA. (C) Student´s T-test shown a decrease of co-localization of Rab7a and Total-Tau in cell cultures treated with siRNA-Rab7a, siRNA-Tau and Nt-siRNA (Pvalue < 0.05 (*), < 0.01 (**), < 0.001 (***)).

V. Discussion

Postmortem cortex and cerebellum´s samples from sCJD-MM1 and sCJD-VV2 patients were examined; we identified significant decreased intracellular levels of endosomal protein Rab9 and an increased intracellular levels of endosomal protein Rab7a in the cortex and cerebellum of human samples from sCJD-MM1 and an increased intracellular levels of Rab7a in the cerebellum of human samples from sCJD-VV2. The increased intracellular levels of Rab7a indicating that specific endosomal network proteins are overexpressed in the specific regions of sCJD-MM1 and sCJD-VV2 patients.

In vivo studies with sCJD of mice showed two stages of the disease, pre-symptomatic and symptomatic, while in humans the only possible stage is symptomatic stage. The increased intracellular levels of Rab7a in the symptomatic and also in pre-symptomatic stage in the brain of mice, suggesting that endosomal protein Rab7a could potentially be used as a sCJD-MM1 and sCJD-VV2 diagnostic biomarker before symptomatic stage settles. In case of sCJD, the presence of Rab7a protein together with other characteristics will allow to make a positive diagnostic. However, studies are required to know if the intracellular levels of Rab7a protein are high in symptoms of the disease in humans.

1 PrP^C and Rab7a/Rab9

Rab7a and Rab9 are located in specific intracellular compartments, late endosome, however the Rab7a protein is also located in lysosomes. Rab7a is the only Rab GTPases protein that is found in lysosome (Hutagalung & Novick 2011). Rab7a regulates membrane traffic from the early endosome to the late endosome and from late endosome to the lysosome for degradation. It is responsible for continuous fusion event between late endosome and lysosomes (Bucci et al. 2000). While, Rab9 protein is involved in the regulation of membrane trafficking between the late endosome and *trans*-Golgi network for recycling (Lombardi et al. 1993).

The cortical neural cell lines from wild type mice showed a significant co-localization between Rab7a and PrP^C than Rab9 and PrP^C. When we transfected

this cells line with siRNA-Rab7a the accumulation of PrP^{C} increased in cytosolic region and their localization was also modified to a punctuated form when compared with control cells. In contrast, the intracellular levels of Rab9 showed no significant regulation in this cell line transfected with siRNA-Rab7a. This data suggests that a great amount of internalized PrP^{C} by endocytosis in normal cells is a target to the degradation pathway and when occurs Rab7a depletion it results in an impairment of PrP^{C} trafficking between early endosome and the late endosome and between late endosome and the lysosome, leading to accumulation of PrP^{C} in the endocytosis pathway. However, the intracellular levels of PrP^{C} is significantly less in cells with Rab7a depletion than in normal cells. This could suggest that PrP^{C} traffic can be made by other endocytosis pathway, for instance, exocytosis when the Rab7a is compromised.

In case of prion disease, the conversion of PrP^{C} to the PrP^{Sc} occurs in the plasma membrane or along the endocytic pathway, before PrP^{Sc} is exposed to endosomal and lysosomal proteases (Caughey et al. 1991). Studies have reported that the majority of PrP^{Sc} is intracellular (Taraboulos et al. 1990), and primarily sequestered with in lysosomes (Godsave *et al.*, 2008; Borchelt, Taraboulos e Prusiner, 1992; Caughey *et al.*, 1991; Marijanovic *et al.*, 2009; McKinley *et al.*, 1991), with little localization at the cell surface (Vey et al. 1996). In our study, we found increased intracellular levels of Rab7a in sCJD MM1 patients, which could suggest an overload of endosomal traffic for degradation. The higher amount of internalized PrP^{C} is a normal target for endocytic pathway and their conversion to PrP^{Sc}, occuring at plasma membrane level or along an endocytic pathway, could suggest that increased intracellular levels of Rab7a is contributing to an accumulation of PrP^{Sc} in lysosomes under the pathophysiological conditions in prion diseases.

2 Total-Tau and Rab7a

Tau proteins belong to the family of microtubule-associated proteins and they provide flexibility and stability to microtubules. Microtubules are responsible for the shape of the cell and serve as tracks for axonal transport (Lodish et al. 2008). Dysfunctions of Tau proteins could possibly lead to increased

phosphorylation and decreased binding to microtubules, ultimately leading to disruption of microtubules (Dixit et al. 2008). Disruption of microtubules changes vesicular biogenesis, vesicle/organelle trafficking, synaptic signaling and it is one of the several neurodegenerative disorders in patients with neurodegenerative diseases (Fletcher & Mullins 2010). Cells lines treated with siRNA-Tau showed significantly increases intracellular levels of Rab7a and Rab9 and alteration of Rab7a localization when Tau is depleted lead to increase dendritic spines.

Neural cortex cell lines from wild type mice showed a significant co-localization between Rab7a and Tau. When we transfected this cells lines with siRNA-rab7a the accumulation of Tau decreases in cytosolic region and their localization was also modified when compared with control cells. These findings suggest that Tau might be degraded after Rab7a depletion.

VI Conclusion

The sCJD MM1, sCJD VV2 and Alzheimer's disease are the most common form of prion disease and neurodegenerative dementia, respectively (Selkoe 1999; Gambetti et al. 2003). Due of the high rate of individuals affected with these diseases worldwide, it is important to develop new knowledge about their pathological features in order to diagnose them in early stage of the disease and develop new treatments before irreversible brain damage occurs. As the fast progressive neurodegeneration (CJD) and slow progressive classical AD are characterized by deposits of aggregated proteins, this accumulation of proteins may activates the protein quality control mechanisms, i.e in the endoplasmic reticulum, the unfolded protein response (UPR). Rab7a which is involved in the retrograde Golgi-ER trafficking and may function as a post-ER quality control system (Hutagalung & Novick 2011), in our study shows an increased intracellular levels of Rab7a in sCJD MM1 and VV2 cases. Thus, our study demonstrate the possible common interactive association of fast progressive and slow progressive neurodegenerative pathway, which the endosomal pathway is more active during fast progressive sCJD MM1, sCJD VV2 than in AD. In conclusion, this study may help to characterize the fast progressive and slow progressive disease, CJD and AD cases. Furthermore, it could be a step forward for the discovery of new biomarkers that could help diagnose the diseases of sCJD and AD before postmortem and also it could be a step ahead to development of new treatment strategies for diseases subtype specific manner.

Bibliography

Aguzzi, A. & Calella, A.M., 2009. Prions: protein aggregation and infectious diseases. *Physiological reviews*, 89(4), pp.1105–1152.

Araújo, A.Q.-C., 2013. Prionic diseases. *Arquivos de neuro-psiquiatria*, 71(9B), pp.731–7. Available at: http://www.ncbi.nlm.nih.gov/pubmed/24141515.

Belay, E.D., 1999. Transmissible spongiform encephalopathies in humans. *Annual Review Of Microbiology*, 53, pp.283 – 314. Available at: http://search.ebscohost.com/login.aspx?direct=true&db=mnh&AN=10547693&site=eds-live [Accessed October 30, 2015].

Bishop, M.T., Will, R.G. & Manson, J.C., 2010. Defining sporadic Creutzfeldt-Jakob disease strains and their transmission properties. *Proceedings of the National Academy of Sciences of the United States of America*, 107(26), pp.12005–10.

Borchelt, D.R., Taraboulos, A. & Prusiner, S.B., 1992. Evidence for synthesis of scrapie prion proteins in the endocytic pathway. *The Journal of biological chemistry*, 267(23), pp.16188–99.

Bucci, C. et al., 2000. Rab7: a key to lysosome biogenesis. *Molecular biology of the cell*, 11(2), pp.467–480.

Cali, I. et al., 2009. Co-existence of scrapie prion protein types 1 and 2 in sporadic Creutzfeldt-Jakob disease: its effect on the phenotype and prion-type characteristics. *Brain : a journal of neurology*, 132(Pt 10), pp.2643–58. Available at: http://www.pubmedcentral.nih.gov/articlerender.fcgi?artid=2766234&tool=pmcentrez&rendertype=abstract.

Cantalupo, G. et al., 2001. Rab-interacting lysosomal protein (RILP): the Rab7 effector required for transport to lysosomes. *The EMBO journal*, 20(4), pp.683–93. Available at: http://www.pubmedcentral.nih.gov/articlerender.fcgi?artid=145419&tool=pmcentrez&rendertype=abstract [Accessed September 8, 2015].

Caughey, B. et al., 1991. N-terminal truncation of the scrapie-associated form of PrP by lysosomal protease(s): implications regarding the site of conversion of PrP to the protease-resistant state. *Journal of virology*, 65(12), pp.6597–603.

Chavrier, P. et al., 1990. Localization of low molecular weight GTP binding proteins to exocytic and endocytic compartments. *Cell*, 62(2), pp.317–329. Available at: http://www.sciencedirect.com/science/article/pii/009286749090369P.

Collins, R.N., 2003. "Getting it on" - GDI displacement and small GTPase membrane recruitment. *Molecular Cell*, 12(5), pp.1064–1066.

Dixit, R. et al., 2008. Differential regulation of dynein and kinesin motor proteins by tau. *Science (New York, N.Y.)*, 319(5866), pp.1086–9.

Dong, J. et al., 2004. The proteasome alpha-subunit XAPC7 interacts specifically with Rab7 and late endosomes. *The Journal of biological chemistry*, 279(20), pp.21334–42. Available at: http://www.ncbi.nlm.nih.gov/pubmed/14998988 [Accessed October 31, 2015].

Fletcher, D.A. & Mullins, R.D., 2010. Cell mechanics and the cytoskeleton. *Nature*, 463(7280), pp.485–492.

Futter, C.E. et al., 2001. Human VPS34 is required for internal vesicle formation within multivesicular endosomes. *Journal of Cell Biology*, 155(7), pp.1251–1263.

Gahan, P.B., 2005. The cell: a molecular approach (3rd edn) G. M. Cooper and R. E. Hausman, Palgrave-Macmillans Global Academic Publishing, 713 pp., ISBN 0-87893-214-3 (2004). *Cell Biochemistry and Function*, 23(3), pp.222–222. Available at: http://doi.wiley.com/10.1002/cbf.1157 [Accessed October 31, 2015].

Gambetti, P. et al., 2003. Sporadic and familial CJD: Classification and characterisation. *British Medical*

Bulletin, 66, pp.213–239.

Grant, B.D. & Sato, M., 2006. Intracellular trafficking. *WormBook : the online review of C. elegans biology*, pp.1–9.

Hanna, J., Carroll, K. & Pfeffer, S.R., 2002. Identification of residues in TIP47 essential for Rab9 binding. *Proceedings of the National Academy of Sciences of the United States of America*, 99(11), pp.7450–7454.

Harris, D. a., 2003. Trafficking, turnover and membrane topology of PrP. *British Medical Bulletin*, 66, pp.71–85.

Hegde, R.S. & Lingappa, V.R., 1999. Regulation of protein biogenesis at the endoplasmic reticulum membrane. *Trends in cell biology*, 9(4), pp.132–137.

Hutagalung, A.H. & Novick, P.J., 2011. Role of Rab GTPases in Membrane Traffic and Cell Physiology. *Physiological Reviews*, 91(1), pp.119–149. Available at: http://physrev.physiology.org/cgi/doi/10.1152/physrev.00059.2009.

Jordens, I. et al., 2001. The Rab7 effector protein RILP controls lysosomal transport by inducing the recruitment of dynein-dynactin motors. *Current Biology*, 11(21), pp.1680–1685.

Kirkpatrick, L.L. & Brady, S.T., 1999. Molecular Components of the Neuronal Cytoskeleton. Available at: http://www.ncbi.nlm.nih.gov/books/NBK28122/ [Accessed October 31, 2015].

Knusel, B. et al., 1990. Selective and nonselective stimulation of central cholinergic and dopaminergic development in vitro by nerve growth factor, basic fibroblast growth factor, epidermal growth factor, insulin and the insulin-like growth factors I and II. *The Journal of neuroscience : the official journal of the Society for Neuroscience*, 10(2), pp.558–70. Available at: http://www.ncbi.nlm.nih.gov/pubmed/2406380 [Accessed October 28, 2015].

Kopke, E. et al., 1993. Microtubule-associated protein tau. Abnormal phosphorylation of a non- paired helical filament pool in Alzheimer disease. *Journal of Biological Chemistry*, 268(18), pp.24374–24384.

Krasnianski, A. et al., 2006. Clinical features and diagnosis of the MM2 cortical subtype of sporadic Creutzfeldt-Jakob disease. *Archives of neurology*, 63(6), pp.876–880.

Ksiezak-Reding, H., Liu, W.K. & Yen, S.H., 1992. Phosphate analysis and dephosphorylation of modified tau associated with paired helical filaments. *Brain research*, 597(2), pp.209–219.

Ladogana, a et al., 2005. Mortality from Creutzfeldt-Jakob disease and related disorders in Europe, Australia, and Canada. *Neurology*, 64(9), pp.1586–91. Available at: http://www.ncbi.nlm.nih.gov/pubmed/15883321.

Laurén, J. et al., 2009. Cellular prion protein mediates impairment of synaptic plasticity by amyloid-beta oligomers. *Nature*, 457(7233), pp.1128–32. Available at: http://www.ncbi.nlm.nih.gov/pubmed/19242475.

Lee, J. et al., 2013. Prion Diseases as Transmissible Zoonotic Diseases. *Osong Public Health and Research Perspectives*, 4(1), pp.57–66. Available at: http://dx.doi.org/10.1016/j.phrp.2012.12.008.

Liemann, S. & Glockshuber, R., 1998. Transmissible spongiform encephalopathies. *Biochemical and biophysical research communications*, 250(2), pp.187–93. Available at: http://www.ncbi.nlm.nih.gov/pubmed/9753605 [Accessed October 31, 2015].

Lin, Z., Zhao, D. & Yang, L., 2013. Interaction between misfolded PrP and the ubiquitin-proteasome system in prion-mediated neurodegeneration. *Acta Biochimica et Biophysica Sinica*, 45(6), pp.477–484.

Llorens, F. et al., 2013. PrP mRNA and protein expression in brain and PrP(c) in CSF in Creutzfeldt-Jakob disease MM1 and VV2. *Prion*, 7(5), pp.383–93.

Lodish, H. et al., 2008. *Molecular Cell Biology*, Available at:

http://www.amazon.ca/exec/obidos/redirect?tag=citeulike09-20&path=ASIN/0716743663.

Lodish, H. et al., 2000a. Molecular Cell Biology. Available at: http://www.ncbi.nlm.nih.gov/books/NBK21475/ [Accessed October 31, 2015].

Lodish, H. et al., 2000b. Molecular Mechanisms of Vesicular Traffic.

Loirand, G., Sauzeau, V. & Pacaud, P., 2013. SMALL G PROTEINS IN THE CARDIOVASCULAR SYSTEM: PHYSIOLOGICAL AND PATHOLOGICAL ASPECTS. *Physiol Rev*, 93, pp.1659–1720.

Lombardi, D. et al., 1993. Rab9 functions in transport between late endosomes and the trans Golgi network. *The EMBO journal*, 12(2), pp.677–682.

Lorca, R. a et al., 2011. The Cellular Prion Protein Prevents Copper-Induced Inhibition of P2X(4) Receptors. *International journal of Alzheimer's disease*, 2011, pp.1–6. Available at: http://www.pubmedcentral.nih.gov/articlerender.fcgi?artid=3202100&tool=pmcentrez&rendertype=abstract.

Manders, E.M. et al., 1992. Dynamics of three-dimensional replication patterns during the S-phase, analysed by double labelling of DNA and confocal microscopy. *Journal of cell science*, 103 (Pt 3, pp.857–62. Available at: http://www.ncbi.nlm.nih.gov/pubmed/1478975 [Accessed October 31, 2015].

Manders, E.M.M., Verbeek, F.J. & Aten, J. a, 1993. Measurement of Colocalization of Objects in Dual-Color Confocal Images. *Journal of Microscopy-Oxford*, 169(January), pp.375–82. Available at: <Go to ISI>://A1993KX70700006.

Martins, V.R. et al., 2010. Prion protein: orchestrating neurotrophic activities. *Current issues in molecular biology*, 12(2), pp.63–86. Available at: http://www.ncbi.nlm.nih.gov/pubmed/19767651 [Accessed September 22, 2015].

Masters, C.L. et al., 1979. Creutzfeldt-Jakob disease: patterns of worldwide occurrence and the significance of familial and sporadic clustering. *Annals of neurology*, 5(2), pp.177–88. Available at: http://www.ncbi.nlm.nih.gov/pubmed/371520 [Accessed September 18, 2015].

McKinley, M.P. et al., 1991. Ultrastructural localization of scrapie prion proteins in cytoplasmic vesicles of infected cultured cells. *Laboratory investigation; a journal of technical methods and pathology*, 65(6), pp.622–30.

Meissner, B. et al., 2005. Sporadic Creutzfeldt-Jakob disease: Clinical and diagnostic characteristics of the rare VV1 type. *Neurology*, 65(10), pp.1544–1550.

Mizuno, D. et al., 2003. Dielectric response in dilute lyotropic lamellar and sponge phases of a nonionic surfactant. *Physical review. E, Statistical, nonlinear, and soft matter physics*, 67(6 Pt 1), p.061505. Available at: http://www.ncbi.nlm.nih.gov/pubmed/16241231 [Accessed October 31, 2015].

Moda, F. et al., 2012. MM2-thalamic Creutzfeldt-Jakob disease: Neuropathological, biochemical and transmission studies identify a distinctive prion strain. *Brain Pathology*, 22(5), pp.662–669.

Moore, R. a., Taubner, L.M. & Priola, S. a., 2009. Prion protein misfolding and disease. *Current Opinion in Structural Biology*, 19(1), pp.14–22.

Mukherjee, S. et al., 2005. Functional analyses and interaction of the XAPC7 proteasome subunit with Rab7. *Methods in enzymology*, 403, pp.650–663.

Nicolas, O., Gavín, R. & Del Río, J.A., 2009. New insights into cellular prion protein (PrPc) functions: the "ying and yang" of a relevant protein. *Brain research reviews*, 61(2), pp.170–84. Available at: http://www.sciencedirect.com/science/article/pii/S0165017309000733 [Accessed October 5, 2015].

Novakofski, J. et al., 2005. Prion biology relevant to bovine spongiform encephalopathy. *Journal of animal science*, 83(6), pp.1455–76.

Padilla, D. et al., 2011. Sheep and goat BSE propagate more efficiently than cattle BSE in human PrP transgenic mice. *PLoS pathogens*, 7(3), p.e1001319.

Parchi, P., Capellari, S., et al., 1999. A subtype of sporadic prion disease mimicking fatal familial insomnia. *Neurology*, 52(9), pp.1757–63. Available at: http://www.ncbi.nlm.nih.gov/pubmed/10371520 [Accessed September 23, 2015].

Parchi, P., Giese, A., et al., 1999. Classification of sporadic Creutzfeldt-Jakob disease based on molecular and phenotypic analysis of 300 subjects. *Annals of neurology*, 46(2), pp.224–33.

Parchi, P. et al., 2009. Incidence and spectrum of sporadic Creutzfeldt-Jakob disease variants with mixed phenotype and co-occurrence of PrPSc types: an updated classification. *Acta neuropathologica*, 118(5), pp.659–71.

Pfeffer, S.R., 2001. Rab GTPases: Specifying and deciphering organelle identity and function. *Trends in Cell Biology*, 11(12), pp.487–491.

Prusiner, S.B., 2004. Detecting mad cow disease. *Scientific American*, 291(1), pp.86–93.

Puoti, G. et al., 2012. Sporadic human prion diseases: Molecular insights and diagnosis. *The Lancet Neurology*, 11(7), pp.618–628. Available at: http://dx.doi.org/10.1016/S1474-4422(12)70063-7.

Resenberger, U.K. et al., 2011. The cellular prion protein mediates neurotoxic signalling of β-sheet-rich conformers independent of prion replication. *The EMBO journal*, 30(10), pp.2057–70. Available at: http://www.pubmedcentral.nih.gov/articlerender.fcgi?artid=3098494&tool=pmcentrez&rendertype=abstract.

Schimmoller, F., Simon, I. & Pfeffer, S.R., 1998. Rab GTPases, Directors of Vesicle Docking. *Journal of Biological Chemistry*, 273(35), pp.22161–22164. Available at: http://www.jbc.org/content/273/35/22161.full [Accessed September 10, 2015].

Selkoe, D.J., 1999. Translating cell biology into therapeutic advances in Alzheimer's disease. *Nature*, 399(6738 Suppl), pp.A23–31. Available at: http://www.ncbi.nlm.nih.gov/pubmed/10392577 [Accessed November 2, 2015].

Stahl, N. et al., 1987. Scrapie prion protein contains a phosphatidylinositol glycolipid. *Cell*, 51(2), pp.229–240.

Stein, M.-P. et al., 2003. Human VPS34 and p150 are Rab7 interacting partners. *Traffic (Copenhagen, Denmark)*, 4(11), pp.754–771.

Takada, L.T. & Geschwind, M.D., 2013. Prion diseases. *Seminars in neurology*, 33(4), pp.348–56. Available at: https://www.thieme-connect.com/products/ejournals/abstract/10.1055/s-0033-1359314 [Accessed October 24, 2015].

Taraboulos, A., Serban, D. & Prusiner, S.B., 1990. Scrapie prion proteins accumulate in the cytoplasm of persistently infected cultured cells. *The Journal of cell biology*, 110(6), pp.2117–32.

Vey, M. et al., 1996. Subcellular colocalization of the cellular and scrapie prion proteins in caveolae-like membranous domains. *Proceedings of the National Academy of Sciences*, 93(25), pp.14945–14949.

Villemeur, T.B., 2013. Creutzfeldt-Jakob disease. *Handbook of clinical neurology*, 112, pp.1191–3. Available at: http://www.ncbi.nlm.nih.gov/pubmed/23622328 [Accessed October 31, 2015].

Wieser, H.G., Schindler, K. & Zumsteg, D., 2006. EEG in Creutzfeldt-Jakob disease. *Clinical Neurophysiology*, 117, pp.935–951.

Wu, M. et al., 2005. Structural basis for recruitment of RILP by small GTPase Rab7. *The EMBO journal*, 24(8), pp.1491–1501.

Zafar, S. et al., 2011. Proteomics approach to identify the interacting partners of cellular prion protein and characterization of Rab7a interaction in neuronal cells. *Journal of proteome research*, 10(7), pp.3123–

35. Available at: http://www.ncbi.nlm.nih.gov/pubmed/21604690 [Accessed October 31, 2015].

Zerial, M. & McBride, H., 2001. Rab proteins as membrane organizers. *Nature reviews. Molecular cell biology*, 2(2), pp.107–117.